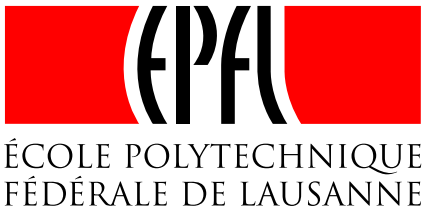


Diploma Report 2005-2006:

# Study of a Quantum Plaquette Model on the Triangular Lattice

Author: **Neftci Emre**
Supervised by Prof. F. Mila, A. Ralko, ITP EPFL

19th December 2005

**Abstract**

In this diploma, we study a Quantum Plaquette Model after we derive its effective hamiltonian starting from the SU(4) symmetric Kugel-Khomskii model which has spin and orbital degrees of freedom. Then we start the numerical approach to the problem. At first, by exact diagonalization, we calculate the energy spectrum which turns out to be degenerate. We suspect that this degeneracy of the ground state is due to the presence of topological sectors, therefore we try to find them and to classify them. We use the preceding information to calculate topological gaps and plaquette to plaquette correlations on lattices up to 588 sites using the Green's Function Monte Carlo algorithm, for which an overview of its basics are given in the appendix. By these means we are able to observe an eventual RVB-liquid state or a long range ordered phase with the plaquette to plaquette correlations.

# Contents

# Chapter 1

# Introduction

Mott insulators with orbital degeneracy have attracted a lot of attention because the orbital degeneracy may have many different consequences, of which some are realized in $LiNiO_2$[5]. It has been suggested that a S=$\frac{1}{2}$ system with double orbital degeneracy, actually has a higher symmetry group than SU(2)×SU(2) which is SU(4) [3]. However never completely realized, the study of SU(4) models can be interesting for some limit cases of the spin orbital model of $LiNiO_2$. The minimal model to describe this SU(4) symmetry is given by the spin-orbital Kugel-Khomskii-like hamiltonian:

$$H = J \sum_{<i,j>} (s_i \cdot s_j + \frac{1}{4})(\tau_i \cdot \tau_j + \frac{1}{4}) \tag{1.1}$$

The $s_i$ describes the spin-$\frac{1}{2}$ degrees of freedom and $\tau_i$ is a pseudo-spin-$\frac{1}{2}$ that describes the orbital degeneracy. For further details concerning the physic of this problem, see [5]. It has been pointed out by *Li et al.*[3], that this hamiltonian has an SU(4) singlet ground state, as we will give an overview in the following paragraphs. The Hamiltonian has been solved on 1D, ladder models and work has been done on 2D models on square lattices [8, 21, 20]. However, before we get into further detail on the plaquette model, let us first give an overview of the frustrated magnetism context.

## 1.1 Frustrated Magnetism and the Heisenberg Model

In frustrated spin models, the energy cannot be independently minimized for each bond and it may either be due to the geometry of the lattice or to competing interactions between the spins, see Fig.1.1. Therefore the ground states of a frustrated *antiferromagnets* may have special structures. Those seen on effective models such as the Quantum Dimer Model(QDM) or the Quantum Plaquette Model(QPM) are some examples.

An example is given by the Heisenberg model which is an effective hamiltonian of the Mott insulator in which each site has spin ↑ or spin ↓ (for a spin $\frac{1}{2}$) having electron hoppings.

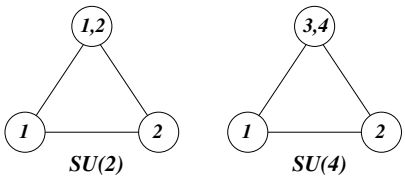


Figure 1.1: The SU(2) model is frustrated due to the geometry of the lattice. On the other hand the SU(4) is not frustrated but is undetermined because of the competing interactions.

The hamiltonian is given by:

$$\mathcal{H}_{Heis} = \sum_{i,j} J_{ij} \boldsymbol{S}_i \cdot \boldsymbol{S}_j \tag{1.2}$$

it is said that this hamiltonian has SU(2) invariance, that is, $\mathcal{H}_{Heis}$ commutes with the operators of SU(2), or more generally with the 3 generators $\{\sigma^i\}$ of the SU(2) group, which is very easy to verify:

$$\sigma^i \mathcal{H}_{Heis} \psi(x) = \mathcal{H}_{Heis} \sigma^i \psi(x) \qquad where \quad S^i = \frac{\bar{h}}{2} \sigma^i \tag{1.3}$$

in other terms, $\mathcal{H}_{Heis}$ and $\sigma^i$ can be simultaneously diagonalized.

## 1.2 From the Quantum Dimer Model to the Quantum Plaquette Model

This study is being done in a similar manner as the Quantum Dimer Model (QDM) [10]. The comprehension of the problem can be made easier if we explain the overview of their work. QDM has been introduced by Rokhsar and Kivelson in order to study the low-energy properties of superconductors. They had argued that in a state with exponential decaying spin-spin correlation with a large excitation gap, the physics was contained in a *Short Range Resonating Valence Bond(SR RVB)* state, spanned by the set of nearest-neighbor valence bond states. These short range valence bonds are called *dimers*. They connect two neighbouring sites to another. The study of the QDM requires many challenging numerical simulations, however in square or triangle lattices, it is possible to have QDM hamiltonians in which the hamiltonian has purely negative off-diagonal elements. Therefore Quantum Monte Carlo is applicable. The QDM hamiltonian can be derived from different models such as $\mathcal{H}_{Heis}$.

As a beginning, one must know that a hardcore dimer (or nearest neighbour valence bond) represents a SU(2) singlet between 2 neighbouring nodes, i.e if a node carries $\frac{1}{2}$-spin degeneracy the singlet is $\frac{1}{\sqrt{2}}(\uparrow\downarrow - \downarrow\uparrow)$, thus the lattice can be covered with them as shown in Fig. 1.2 . This model has been thoroughly studied in the square lattice , the triangular lattice[13] and on some more specific lattices such as the kagomé and the honeycomb lattice[22, 2, 4, 6].

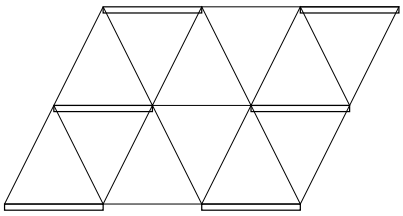

Figure 1.2: Dimer coverings of the triangular lattice

Now let us turn to our problem, which remains unstudied for the moment: the low-energy states of an SU(4) model consists of a plaquette covering of the lattice as argued by Li[3]. In fact, in this paper it has been shown that in the case of the triangular lattice the average energy per bond of a plaquette covering is lower than any other valence bond state or a classical Néel state.

By following the QDM scheme, we wish to create a Quantum Plaquette Model (QPM) which consists of plaquette coverings of the lattice, see Fig. 2.3. We will generalize the SU(2) invariant model to a SU(4) invariant model, i.e the hamiltonian will commute with the 15 generators of SU(4) (in general the SU(N) group has $N^2-1$ generators).

The SU(N) invariant hamiltonian for a nearest-neighbour model that reminds us $\mathcal{H}_{Heis}$can be written:

$$\mathcal{H} = \sum_{<i,j>} J\, S^n_m(i) S^m_n(j) \tag{1.4}$$

where $S^n_m(i)$ is a generator of SU(N) and the $n, m$ indexes are summed and $J > 0$ for an anti-ferromagnetic case. The case of $N = 4$ is the most studied except for the SU(2) model and from now on we will restrict ourselves to this case.

On the other hand, the full symmetry of eq. (1.1) is the SU(4) symmetry group which unifies the spin and the pseudo-spin (orbital) degrees of freedom. Let us prove it. We can write eq.(1.1) in a manner that explicits SU(4) symmetry and that gives an intuitive link to the preceding SU(4) Heisenberg-like Hamiltonian eq.(1.4) [3]:

$$\mathcal{H} = \sum_{<i,j>} (\sum_{\gamma=1}^{15} A^\gamma_i A^\gamma_j + 1) \tag{1.5}$$

The $A^\gamma_i$ operators are $2s^\alpha$,$2\tau^\alpha$ and $4s^\alpha\tau^\beta$, where $s^\alpha$ notes the standard spin-$\frac{1}{2}$ operator and $\tau^\alpha$ an orbital pseudo-spin-$\frac{1}{2}$ operator and $\alpha, \beta = x, y, z$. Eq. (1.5) acts on a Hilbert space of the 4 following basis states, consisting in a standard spin and an orbital spin state: $|\pm\frac{1}{2}, \pm\frac{1}{2}\rangle$. These vectors span a fundamental representation of the SU(4) group. Both operators $s$ and $\tau$ can be expressed in terms of $S^n_m$ since themselves can be expressed in terms of creators: $S^n_m(i) = c^\dagger_{i,m} c_{i,n}$ where $i$ is the site and $m, n$ the state. Now is clear the eq. (1.5) has SU(4) symmetry since the $S^n_m$'s are generators of SU(4).

The four site ground state of the preceding hamiltonian is a unique SU(4) singlet, which is by definition invariant by application of SU(4) operators. We will call this singlet a plaquette. A SU(4) singlet can be written in terms of an antisymmetric sum of fermion creators:

$$|S\rangle = \frac{1}{\sqrt{24}} \sum_{\{i,j,k,l\}} c_{i_1}^\dagger c_{j_2}^\dagger c_{k_3}^\dagger c_{l_4}^\dagger |0\rangle \tag{1.6}$$

where $|0\rangle$ is the vacuum state and the sum is a permutation of the $\{i, j, k, l\}$ elements. The resulting state is antisymmetric. As mentioned before, the energy of a plaquette state has the lowest energy amongst the other possible valence bond states.

## 1.3 Phases and Transitions

In the case of the Quantum Dimer Model (QDM) on the triangular lattice, different phases have been numerically pointed out by *Moessner and Sondhi*[9] and *Ralko et al.*[10] ranging from the columnar, $\sqrt{12} \times \sqrt{12}$ to the RVB-liquid and the staggered states. The transition between these phases occurs at certain values of a parameter that have been determined. Theses phases are characterized by topological properties: a phase may only consist in configurations that are in certain *topological sectors (TS)*. A topological sector is a sub-Hilbertspace whose vectors are connected via successive applications of the hamiltonian. They define quantities which are invariant by local moves caused by the application of $H_{QPM}$.

In the case of dimers on the triangular and the square lattices, the topological sectors are uniquely classified by numbers which are the winding numbers, i.e number of loops around the torus depicted by *transition graphs[11]*. Finding such topological sectors, and especially an efficient way to classify them, is extremely helpful and will be a milestone of the research on the QPM.

The following presents an example of what information the TS may give: if two phases consist in sets of configurations lying in different topological sectors, we may study the transitions in terms of topological gaps $\Delta = |E_{TS_1} - E_{TS_2}|$ where $E_{TS_i}$ are the ground state energies in topological sector $i$. If a topological gap closes for certain value of the parameter, there will be a possible phase transition. We will see that an efficient way to classify the configurations in the TS is the only way to observe such gaps on very large clusters, where we do not have access to the full Hilbert space. Note that these transitions may be either first order-like or second order-like. Finding the phases and the eventual boundary values of the parameter will be the other issue in this diploma.

## 1.4 Deriving the Quantum Plaquette Model Hamiltonian

But before we start looking for topological sectors and studying the transitions, let us formally derive an effective hamiltonian for our model. This hamiltonian

has been fully derived by *Penc et al.* [8]. It has been suggested in [15, 16] that different configurations may be connected by local permutations of some plaquettes, which we will call a *diamond flip*. The lowest order local permutations are depicted on Fig. 1.3.

But first, let us start from the SU(4) invariant Hamiltonian. As said before we suppose that the low-energy physics are well described by solutions consisting of plaquette coverings. Thus, we shall restrict ourselves to the subspace of these coverings that we note $\{|\psi_i\rangle\}$. However, this set is not an orthogonal one. In fact we can define an overlap matrix which has non-zero off-diagonal elements:

$$O_{ij} = \langle\psi_i|\psi_j\rangle \tag{1.7}$$

The demonstration of the effective hamiltonian will proceed in the following steps:

- Calculation of the overlap matrix
- Calculation of $\langle\psi_i|H|\psi_j\rangle$, where $H$ is the initial hamiltonian defined in eq. (1.4)
- Orthogonalization of the basis $\{|\psi_i\rangle\}$
- Matrix element calculation of the effective hamiltonian $H_{QPM}$

### 1.4.1 Calculation of the Overlap Matrix:

Let us write the SU(4) singlets in eq. (1.6) with the Levi-Civita symbol:

$$|[a,b,c,d]\rangle = \frac{1}{\sqrt{24}} \sum_{i_a=1}^{4}\sum_{i_b=1}^{4}\sum_{i_c=1}^{4}\sum_{i_d=1}^{4} \varepsilon_{i_a i_b i_c i_d}|i_a i_b i_c i_d\rangle \tag{1.8}$$

From now on, when closed in brackets, the letters/numbers refer to the sites. It is reminded that the levi civita symbol is the fully antisymmetric tensor, more explicitly defined by:

$$\varepsilon_{i_a i_b i_c i_d} = \begin{cases} 0 & \text{if any of the two labels are the same} \\ 1 & \text{if the labels are an even permutation of (1, 2, 3, 4)} \\ -1 & \text{if the labels are an odd permuation of (1, 2, 3, 4)} \end{cases}$$

where $\{1,2,3,4\}$ refers to the different spin pseudo-spin vectors $\{|\pm\pm\rangle\}$ on each site. To calculate the overlap, we have to compute the expressions of the following type (using the Einstein summing convention on repeated labels):

$$\langle j_a j_b j_c j_d|\varepsilon^{j_a j_b j_c j_d}\varepsilon_{i_a i_b i_c i_d}|i_a i_b i_c i_d\rangle$$

By a straightforward calculation, we find that singlets sharing two sites $m, n$ have an overlap:

$$\varepsilon^{j_a j_b n\, m}\varepsilon_{i_a i_b n\, m} = 2\cdot(\delta^{j_a}_{i_a}\delta^{j_b}_{i_b} - \delta^{j_a}_{i_b}\delta^{j_b}_{i_a})$$

and singlets sharing three sites $m, n, o$ have an overlap:

$$\varepsilon^{j_a o n m}\varepsilon_{i_a o n m} = 6 \cdot \delta^{j_a}_{i_a}$$

Now, let us calculate the overlap of the lowest resonance depicted on Fig. 1.3. Between two configurations $i$ and $j$ that differ by such flip, it is given by:

$$O_{ij} = \langle [1\,2\,3\,4][6\,7\,10\,11][5\,8\,9\,10]|[1\,2\,4\,5][3\,6\,7\,10][8\,9\,11\,12]\rangle$$

$$\begin{aligned} &= \frac{1}{24^3}\varepsilon^{i_1 i_2 i_3 i_4}\varepsilon_{i_1 i_2 i_4 i_5}\varepsilon^{i_6 i_7 i_{10} i_{11}}\varepsilon_{i_3 i_6 i_7 i_{10}}\varepsilon^{i_5 i_8 i_9 i_{12}}\varepsilon_{i_8 i_9 i_{11} i_{12}} \\ &= \frac{1}{24}\cdot\frac{3}{8}\cdot\delta^{i_3}_{i_5}\delta^{i_5}_{i_{11}}\delta^{i_{11}}_{i_3} \\ &= \frac{1}{16} \end{aligned}$$

### 1.4.2 Calculation of the Matrix Elements of the Hamiltonian in the Original Basis

Now, we want to calculate the matrix elements of the effective hamiltonian in the configurations basis $\{|\psi\rangle\}$, defined as:

$$H_{ij} \equiv \langle\psi_i|H|\psi_j\rangle$$

We remind that $|\psi_i\rangle$ are SU(4) singlets which can be written in terms of spin and chirality vectors which are one of the four possibilities $|+-\rangle$, $|++\rangle$, $|-+\rangle$, $|--\rangle$. Therefore, each plaquette is a sum of 24 terms. A cluster has $\frac{N}{4}$ plaquettes, hence a configuration is a tensorial product of $\frac{N}{4}$ different singlets having each 24 terms. This calculation is very long and it has been done by *Penc et al.* [16, 8]. The result is the following:

$$H_{ij} = \varepsilon(\delta_{ij} + \alpha A_{ij}) \tag{1.9}$$

where $\varepsilon$ is the energy of the SU(4) singlet. The average energy per bond is $-\frac{13}{48}$ [3], and there are 12 satisfied bonds per plaquette and $\frac{N}{4}$ plaquettes on an $N$-site cluster. So the energy is $\varepsilon = -J\,N\cdot\frac{13}{4}$. Eq. (1.9) is the key point of the derivation of the QPM since it involves simply the overlap matrix: $H_{ij} = \varepsilon O_{ij}$. It will prove to be extremely helpful to compute the terms of our effective hamiltonian as we shall see in a few paragraphs.

### 1.4.3 Orthogonalization of the Basis

We can formulate the overlap matrix $O_{ij}$ in the following manner:

$$O_{ij} = \delta_{ij} + \alpha A_{ij} + \beta B_{ij} + ... \tag{1.10}$$

where $A_{ij}$ is the matrix element corresponding to 2 configurations that differ by a diamond-loop, $B_{ij}$ the matrix elements of a higher order loop, and $\alpha = \frac{1}{16}$ the overlap value calculated in Sec. 1.4.1. Note that $\sum_k A_{ik} = N_d$ counts the

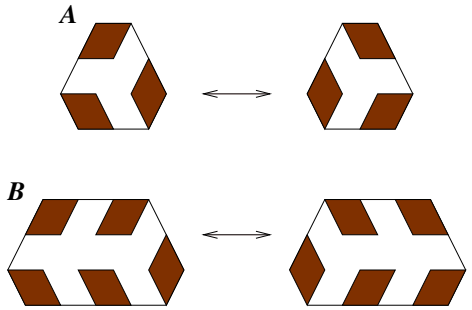


Figure 1.3: The two lowest loop resonances on the plaquette model. For A) only 3 plaquettes are concerned, hence this permutation (or flip) will be much more probable than the B) flip. For these obvious reasons, the situation in A) will be the only one considered in $H_{QPM}$ and we will call it a *diamond* flip.

number of diamonds on configuration $i$.
Higher order loops involve overlap values which are of higher order in $\alpha$. A first approach in our QPM consists in neglecting them.

The overlap matrix $O$ limited to the simplest resonance is approximated by:

$$O_{ij} \cong \delta_{ij} + \alpha A_{ij} \tag{1.11}$$

We define a set of orthogonal states $\{|\tilde{\psi}_i\rangle\}$by:

$$|\tilde{\psi}_i\rangle = \sum_k O_{ik}^{-\frac{1}{2}} |\psi_k\rangle \tag{1.12}$$

Since, by construction,

$$\begin{aligned} \langle\tilde{\psi}_i|\tilde{\psi}_j\rangle &= \sum_{l,k} \langle\psi_l| O_{il}^{-\frac{1}{2}} O_{jk}^{-\frac{1}{2}} |\psi_k\rangle = \sum_{l,k} O_{il}^{-\frac{1}{2}} O_{jk}^{-\frac{1}{2}} O_{lk} \\ &= \sum_k O_{jk}^{-\frac{1}{2}} (O^{-\frac{1}{2}} O)_{ki} \\ &= \delta_{ij} \end{aligned}$$

where we have used the symmetry of the overlap matrix. We may write an approximated $O^{-\frac{1}{2}}$, for $\alpha$ small:

$$O^{-\frac{1}{2}} \cong \mathbb{I} - \frac{1}{2}\alpha A \tag{1.13}$$

Now the new vectors are:

$$|\tilde{\psi}_i\rangle = \sum_k (\delta_{ik} - \frac{1}{2}\alpha A_{ik})|\psi_k\rangle = |\psi_i > -\frac{1}{2}\alpha \sum_k A_{ik}|\psi_k\rangle$$

### 1.4.4 Calculation of the Effective Hamiltonian

The effective hamiltonian arises by calculating its elements in the new basis:

$$(\tilde{\mathcal{H}}_{QPM})_{ij} = \langle\tilde{\psi}_i|H|\tilde{\psi}_j\rangle = (\langle\psi_i| - \frac{1}{2}\alpha\sum_k A_{ik}\langle\psi_k|)\, H\, (-\frac{1}{2}\alpha\sum_l A_{jl}|\psi_l\rangle + |\psi_j\rangle)$$

By neglecting terms of order higher than $\alpha^2$, we get:

$$\begin{aligned}(\tilde{\mathcal{H}}_{QPM})_{ij} &= \langle\psi_i|H|\psi_j\rangle - \frac{\alpha}{2}\sum_k\langle\psi_k|A_{ik}H|\psi_j\rangle - \frac{\alpha}{2}\sum_l\langle\psi_i|A_{jl}H|\psi_l\rangle + ... \\ &= \langle\psi_i|H|\psi_j\rangle - \frac{\alpha}{2}\sum_k(A_{ik}\langle\psi_k|H|\psi_j\rangle + A_{jk}\langle\psi_k|H|\psi_i\rangle) \\ &= C^{te} + \tilde{H}_{ij} - \frac{\alpha}{2}\sum_k A_{ik}\tilde{H}_{kj} + A_{jk}\tilde{H}_{ki} \qquad (1.14)\end{aligned}$$

The passage from the first line to the second line is justified by the fact that $H$ and $A$ are symmetric, whereas we rename the dummy variable $l$ to $k$. In the last line we have removed the constant part of $H_{ij}$, namely: $\tilde{H}_{ij} = H_{ij} - \varepsilon\delta_{ij}$. We replace $H_{ij}$ with its expression from eq. (1.9), then eq. (1.14) becomes:

$$(\tilde{\mathcal{H}}_{QPM})_{ij} = \varepsilon\alpha A_{ij} - \alpha^2\varepsilon\sum_k A_{ik}A_{kj}$$

The next step deserves some explanation. Three possibilities are offered to $\sum_k A_{ik}A_{kj}$:

1. $|\psi_i\rangle$ and $|\psi_j\rangle$ differ by **no loops:** In other words, $|\psi_i\rangle = |\psi_j\rangle$ and $A_{ik}^2 = A_{ik}$ since its elements are either 1 or 0. Hence we get the only contributing term: $\sum_k A_{kj} = N_d(i)$, where $N_d(i)$ is the number of diamonds in the configuration $i$.

2. $|\psi_i\rangle$ and $|\psi_j\rangle$ differ by **one loop**: In this case $\sum_k A_{ik}A_{kj}$ becomes $\sum_{k_i}^{N_d(i)} A_{k_ij}$, it is understood that $k_i$ refers to all configurations connected by a diamond flip. Since $i$ and $k$ differed by one loop, $j$ must not differ by a loop with $k$. Hence this sum is always zero.

3. $|\psi_i\rangle$ and $|\psi_j\rangle$ differ by **two loops**: This is the trickiest case. At first, the sum becomes $\sum_{k_i}^{N_d(i)} A_{k_ij}$. Again, $j$ must differ by one loop from $k_i$. This is only possible if $j = k_i$. Since $A_{ij}$ has no diagonal elements, this sum is equal to zero.

Therefore our effective hamiltonian finally becomes:

$$(\tilde{\mathcal{H}}_{QPM})_{ij} = \varepsilon\alpha A_{ij} - \alpha^2\varepsilon N_d(i)\cdot\delta_{ij} \qquad (1.15)$$

The first term of eq. (1.15) contributes when $i$ and $j$ differ by one loop. It is the off diagonal part of the hamiltonian and it implements the dynamics of the

model. The second term is the diagonal potential term: it simply counts the number of permutable items and leaves the state unchanged. We may rewrite eq. (1.15) it in the following manner:

$$H_{QPM} = \sum_{Diamond} (V\,\mathbb{V} - t\,\mathbb{K}) \tag{1.16}$$

where $\mathbb{V}$ is the potential term and $\mathbb{K}$ the kinetic term and $V$, $t$ respectively equal to 1 and 16 for our effective model, and $\frac{V}{t}$ is the parameter of our model. In fact, in these effective models, one can modulate this parameter since the hamiltonian is only an approximation of reality. Roughly speaking, if $\frac{V}{t} > 1$, configurations having a lot of flippable plaquettes will have higher energy. On the other hand they will be favoured if $\frac{V}{t} < 1$ .

Instead of giving an interpretation of the $\{|\tilde{\psi}\rangle\}$, it is better to consider that the new hamiltonian is a unitary transformation of the first hamiltonian, namely $H_{QPM} = O^{\frac{1}{2}^{-1}} \cdot H \cdot O^{\frac{1}{2}}$ while still working with the original basis $\{|\psi_i\rangle\}$ which are the plaquette configurations. Schematically, the $H_{QPM}$ looks like this:

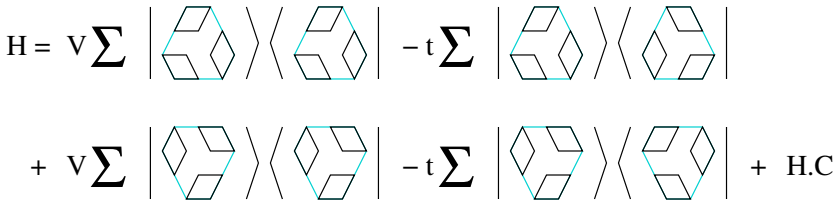


where the sums run over all the flippable diamonds.

# Chapter 2

# Finding the Hilbert Spaces

The second step of this study is to generate numerically the Hilbert space in which the effective hamiltonian is defined, or in other words, all the possible close-packed plaquette states.
In order to find these Hilbert spaces, it is necessary to write down a program that will build up these configurations. It is impossible to calculate the Hilbert space for $N_{sites} > 48$ but we must keep in mind that these finite-size clusters will only help us to find the properties in the thermodynamic limit. In the infinite triangular lattice, a symmetry group which leaves the sites and the neighbours invariant is the translation group ( generated by the two unit vectors $\mathbf{u}, \mathbf{v}$ as described below) times the point group ($\pi$ and $\frac{2\pi}{3}$ Rotations, inversions on the $\mathbf{u}$ axis). In order to have finite lattices which have the same symmetries, we apply periodic boundary conditions. Unfortunately, not all lattices can verify these conditions, and we shall see both possibilities in the following section. See appendix of [7] for further details.

A program that we have written builds all the possible configurations in a recursive way. See Fig. 2.1 for a brief view of its steps.

## 2.1 Clusters on the Triangular Lattice

For this type of lattice, each node has six neighbours. $\boldsymbol{u}$ and $\boldsymbol{v}$ are the two primary vectors of the lattice and are defined as:

$$\boldsymbol{u} = 1 \cdot \boldsymbol{x} + 0 \cdot \boldsymbol{y} \tag{2.1}$$

$$\boldsymbol{v} = \frac{1}{2} \cdot \boldsymbol{x} + \frac{\sqrt{3}}{2} \cdot \boldsymbol{y} \tag{2.2}$$

We now define the translation vectors of the lattice that sets the periodicity of the lattice. We call them $\boldsymbol{T}_1$ and $\boldsymbol{T}_2$. Let $\boldsymbol{p} = (u, v)$ be a position in the lattice. Then accordingly to the definition of $\boldsymbol{T}_1$ and $\boldsymbol{T}_2$:

$$\boldsymbol{p} + n\boldsymbol{T}_1 + m\boldsymbol{T}_2 = \boldsymbol{p} \qquad n \in \mathbb{N}, m \in \mathbb{N} \tag{2.3}$$

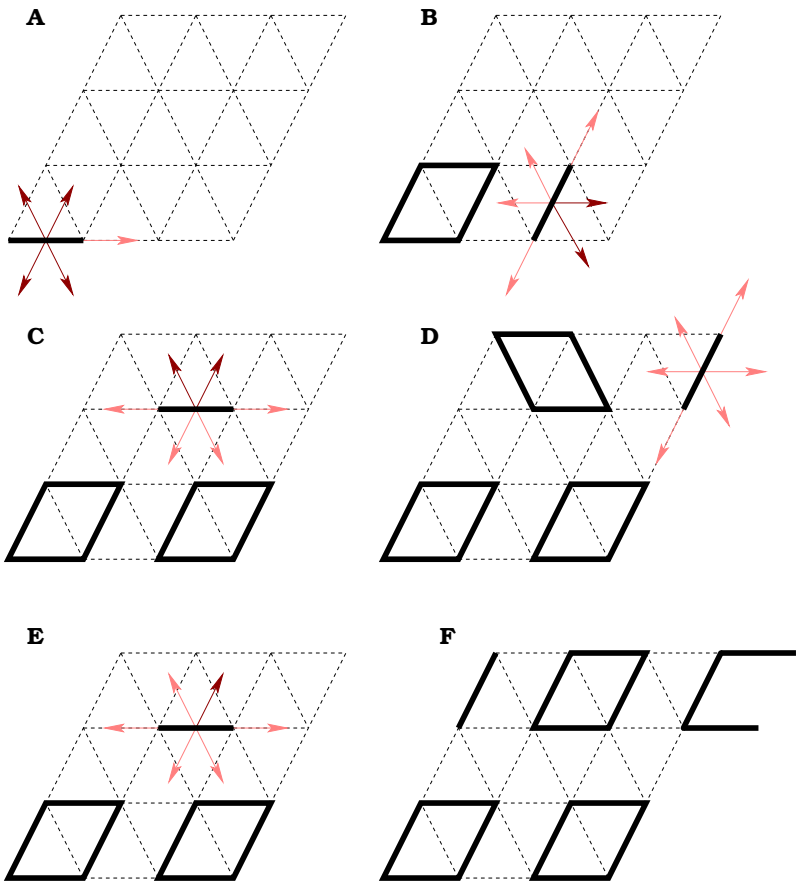


Figure 2.1: This figure shows the steps of the plaquette covering function. A) An occupied link is chosen. The program looks to translate the link in a valid direction (i.e an unoccupied link, its direction is indicated by the dark arrows). Once the link is found, the plaquette is built. B) Another link is chosen and a plaquette is built in one of the valid directions (chosen arbitrarily)C) Same as B), note that there are two valid directions. D) There are no valid directions therefore no plaquette can be built anymore. If this configuration did not contain any "holes" it would form a $|\psi_i\rangle$ configuration. E) The function returns to its last step, destroys the previous plaquette and chooses the another valid direction in C). F) A new close-packed configuration is found, and forms $|\psi_i\rangle$ and so on. This way, all the Hilbert space of close-packed configurations is spanned.

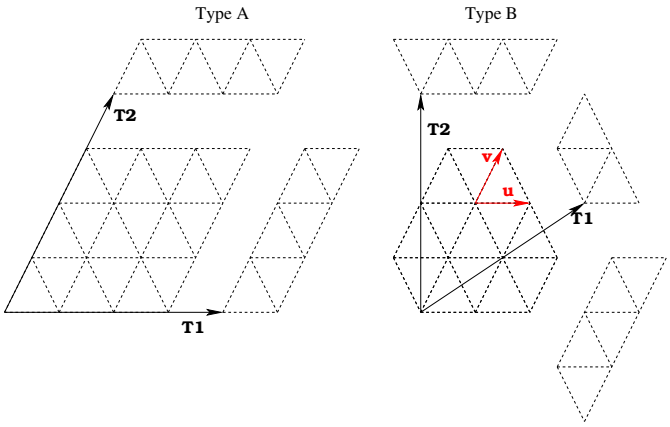


Figure 2.2: Type A and type B clusters for the triangular lattice

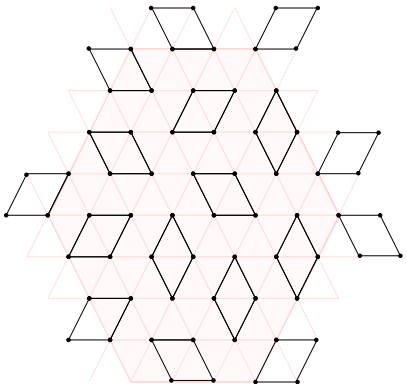

Figure 2.3: A plaquette configuration on the N=48 Type B lattice

Considering the comments in the first paragraph, the only two clusters that verify the symmetries of the infinite triangular lattice are defined by:

$$\boldsymbol{T}_1 = l \cdot \boldsymbol{u} + m \cdot \boldsymbol{v} \quad (2.4)$$

$$\boldsymbol{T}_2 = -m \cdot \boldsymbol{u} + (l+m) \cdot \boldsymbol{v} \quad (2.5)$$

with $l$ or $m = 0$ for the first type (A) and $l = m$ for the second type (B). Both types are shown in Fig. 2.2. An example of a 48-site plaquette covering is given on Fig.2.3. The relation between N, the number of sites, and $l, m$ is simply given by: $N = l^2 + lm + m^2$.

Since we are looking for clusters that will accommodate a plaquette covering without free nodes, the possible N's are multiple of four only: 12 (B), 16(A), 36(A), 48(B). Past 48, the calculation time and the required memory is far too large. The dimension of the Hilbert space grows exponentially as seen on Fig. 2.4. Finally, Tab. 2.1 lists the size of the Hilbert spaces for the chosen N's. According to the fit, the next cluster which might interest us, i.e $N = 108$ will have a Hilbert space whose dimension is in the order of $10^7$. Unfortunately,

| $N$ | $Z$ |
|---|---|
| 12 | 36 |
| 16 | 96 |
| 36 | 540 |
| 48 | 3900 |

Table 2.1: Size of the Hilbert space for some finite-size lattices

even if we find the Hilbert space, it will be impossible to proceed to exact diagonalization even with advanced methods such as Lanczos.

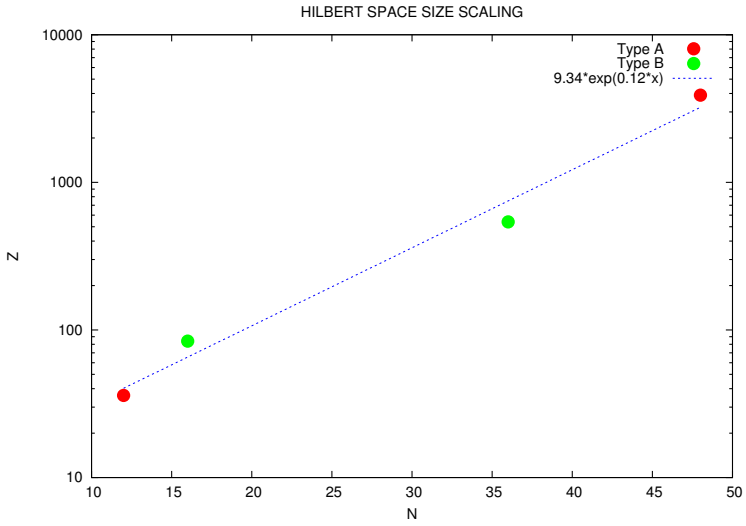


Figure 2.4: Z(N) is the size of the Hilbert space. Due to the different boundary conditions between the different types of clusters, it is possible that Z(N) grows differently for each type. However, no conclusion can be taken since we have only two data points for each type. The values are presented in Tab. 2.1

# Chapter 3

# Numerical Study by Exact Diagonalization

In the previous section, we have found the entire Hilbert space of some clusters. Although these clusters are small compared to what we are interested in, which is the thermodynamic limit, they will prove to be very useful to get a greater understanding of the situation.

By using exact diagonalizations, we have found the full spectrum for the 12-site, 36-site and 48-site clusters. The 16-site is not a multiple of 12, therefore it is not interesting for further study because it cannot accommodate diamonds in a close-packed manner. From now on, we will restrict ourselves to clusters having a number of sites being a multiple of 12.

The configurations are coded by sites. On each site number we assign a number which defines one of the twelve plaquettes which can be built around it. We make all possible diamond flips according to the QPM hamiltonian and we find it's matrix elements. We now have a table of all elements of our symmetric hamiltonian and we diagonalize it. Clusters having over 48 sites are difficult to solve in this manner because of the required memory.

## 3.1 Energy Spectrum of the QPM

One might notice that there are no level crossings on the spectrum. Therefore we suspect that there are no first order phase transitions at $\frac{V}{t} < 1$. The slope of the 12-site total energy in function of $\frac{V}{t}$ is -2, corresponding to the number of flippable items on such a cluster.

We vary $\frac{V}{t}$ around -2 (favouring configurations having flippable diamonds) to 2 (favouring configurations having no flippable plaquettes). Spectra of the 12-site, 36-site and 48-site clusters are represented on Fig. 3.1. An observation of the eigenvectors shows us different phases by varying the parameter $\frac{V}{t}$:

- $\frac{V}{t} > 1$: the ground state is highly degenerate and is formed by the columnar configurations, i.e by definition configurations having no flippable diamonds[1]. In fact, both terms of the hamiltonian cancel since there are

[1] Beware of the confusion with the dimer model whereas the columnar state is, by opposi-

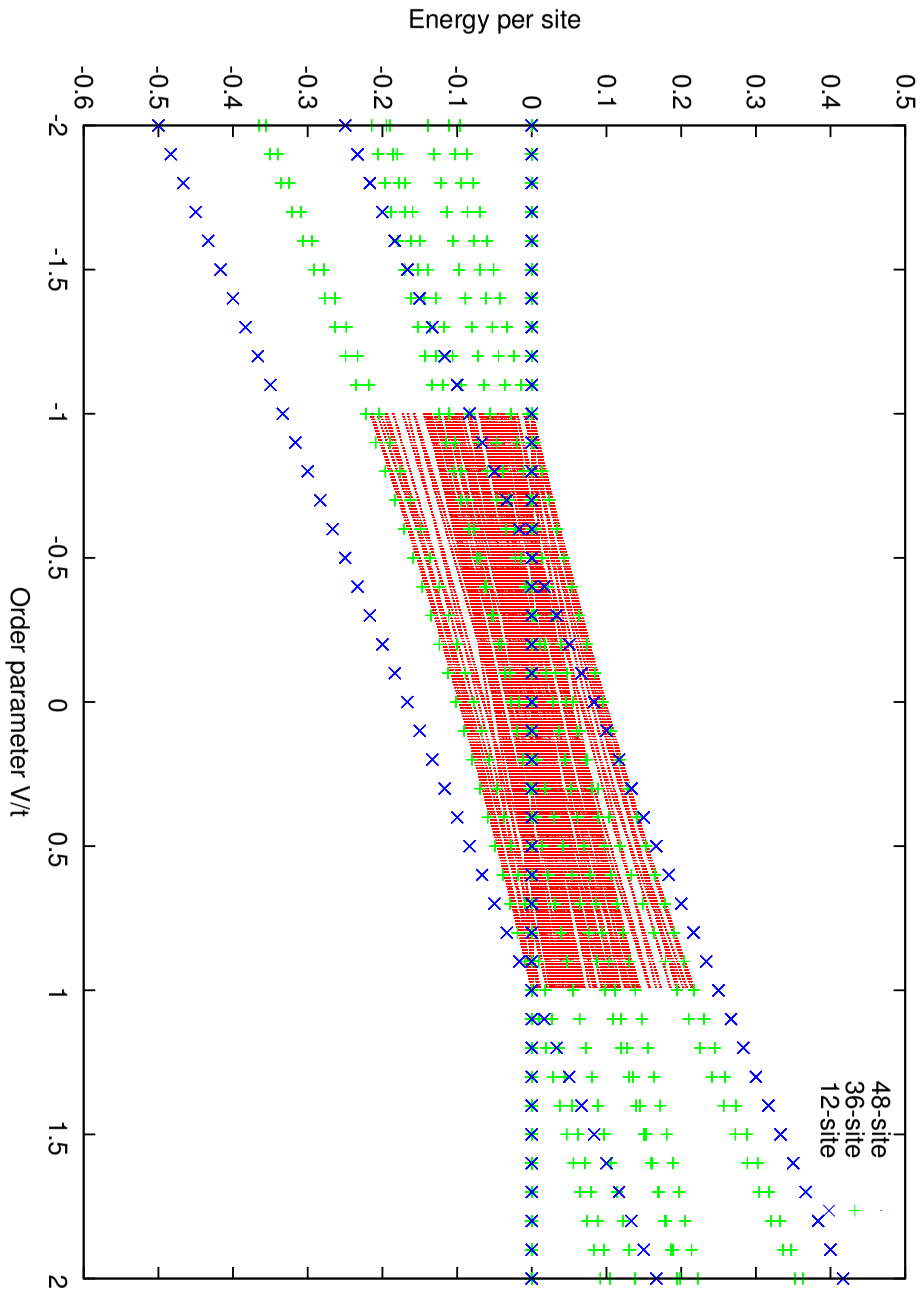


Figure 3.1: Energy spectra by exact diagonalization for the 12-site, the 36-site and the 48-site cluster. Note that the ground state changes abruptly at $\frac{V}{t} = 1$. The increasing levels for each cluster are the excited states.

no flippable items therefore no contributions to the energy. The degeneracy is equal to the number of topological sectors consisting in only one state (which reduces to singles configurations). They are the *staggered* configurations in this model.

- $\frac{V}{t} = 1$: which is called the RK point is possibly a short range RVB-liquid state [11]. At this point, the ground state has zero energy. The degeneracy is equal to the number of different topological sectors.
  In fact, at this point, as is the case with the dimer problem on the square lattice [11], we have verified that each topological sector has a non-degenerate ground state $|\Psi>$ which is an equally weighted superposition of all the configurations in that sector.

$$|\Psi\rangle = \frac{1}{\sqrt{N_{TS}}} \sum_p |c_p\rangle$$

  where $N_{TS}$ is the number of states in that sector.
  Considering this fact, it is easy to understand why the energy is equal to zero. Both potential and kinetic terms cancel each other because any new configuration generated by the kinetic term has his opposite term coming from the potential, hence all contributions cancel since $V = t$.

- $\frac{V}{t} \leq 1$: the ground state ceases to be generated by the totally unflippable configurations and become mixed, with a trend to states having flippable diamonds.

- $\frac{V}{t} \ll 1$: the ground states consist in the maximally flippable configurations, which is in accordance with the hamiltonian.

At $V < 1$, the ground states of both 12-site and 36-site clusters are 8-fold degenerate, and 20-fold degenerate for the 48-site. The degeneracy of the ground state is likely due to the presence of topological sectors which have the same energy. We will investigate them in Chap. 4.

To convince ourselves qualitatively of the preceding facts, an interesting quantity to observe is the mean value of the *number of diamonds operator* $N_d$ for a given $\frac{V}{t}$ in a certain state, or more explicitly:

$$N_d(i) = \langle\psi_i|N_d|\psi_i\rangle = \sum_p n_d(p)|\alpha_{ip}|^2$$

where $|\psi_i\rangle = \sum_p \alpha_{ip}|c_p\rangle$ are the eigenvectors of the hamiltonian, $|c_p\rangle$ a plaquette configuration, and $n_d$ the number of diamonds in $|c_p\rangle$. Fig. 3.2 shows $N_d(i)$ for each $|\psi_i\rangle$ of the ground state.

tion, the states that have a maximum number of flippable entities.

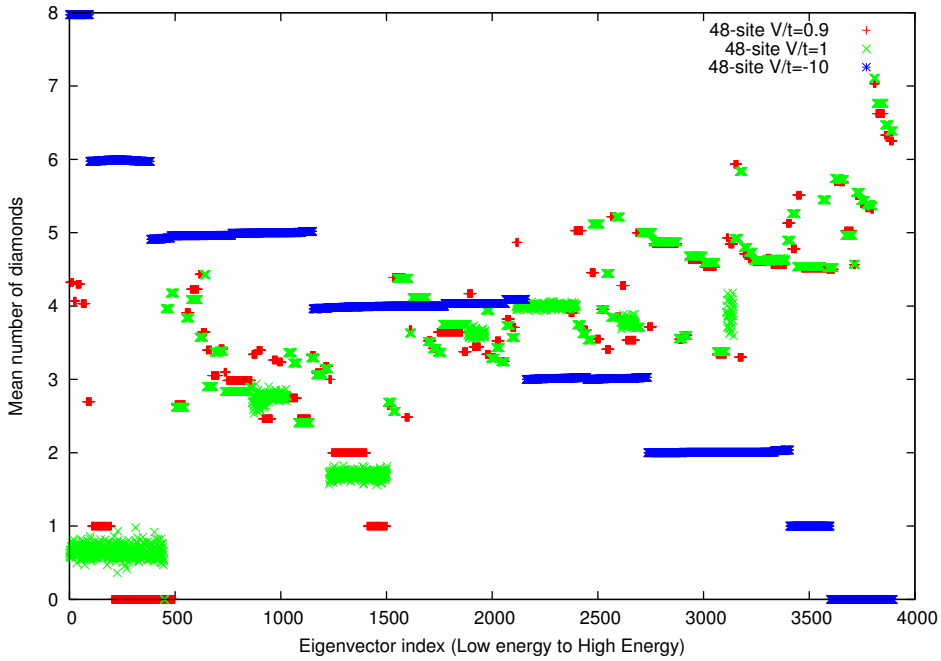


Figure 3.2: The mean number of diamonds for each eigenvector, which are indexed from low to high energy. One can easily see the effect of the hamiltonian between $\frac{V}{t} = -10$ and $\frac{V}{t} = 1$. And possibly an RVB-liquid state for $\frac{V}{t} = 1$ where the 48-site cluster is 452 times degenerate.

# Chapter 4

# Topological Sectors

## 4.1 Results Obtained by Exact Diagonalization

In order to emit a full characterization of the QPM and to get clues about the different phases, the notion of Topological Sectors (TS) is extremely useful. By definition, a topological sector is a sub-Hilbertspace in which the vectors are connected via successive applications of the hamiltonian. A TS can be the entire Hilbert space, in which case its introduction is useless. However in quantum dimer models on a triangular lattice, for example, if we exclude the staggered configurations, there are 4 TS , i.e four sets of vectors that cannot be obtained one another with $H$. In that model, one can obtain precious information thanks to the topological gaps, which is the difference between the ground state energy of one topological sector from another. Therefore they can give us some information about the phase transitions, be there any. At last, a good understanding of the TS i.e possibility to generate any configuration in the desired TS, is extremely helpful for the Green's Function Monte Carlo on very large clusters ($N > 100$).

In our case, we will see that we have much more TS than the triangular lattice. We have not been able to give a full characterization of them in the general case, although we have emitted some clues. However, we have well characterized the fully flippable configurations and possibly it's first "excited" TS.

In order to get a clue of these TS, we have first used the ergodicity property to find the number of disconnected subspaces, the number states each one contains. In other words, after successive applications of $H$ on the states that we have found in Chap. 2, we get a partition of the states.

The results are as follows:

- **12-site** and **36-site:** There are 2 types of subspaces: one containing only one state (no diamonds) and another containing one or more diamonds (From now on, we will call these types of subspaces *super-blocks*). Both clusters had 8 of such subspaces which was not surprising according to the degeneracy of the ground state, as we have found before.

- **48-site:** This case was more surprising since we found 2 sets of different

blocks (super-blocks) that had the same energy, one having 8 subspaces and the other 12 subspaces, containing respectively 57 and 114 states, adding to 20 which was the degeneracy of the ground state, as seen in Chap. 2. It also contained 12 96-state sectors, 24 18-state sectors and 96 2-state sectors. From now one we will write them as $TS_N$, where $N = 114, 57, 96, 18, 2, 1$ respectively. We have computed the ground state energy in each of the TS (i.e simple diagonalization of H restricted to the states in each TS). The results were the following: all the eigenstates of one subspace are non-degenerate and the ground state energy (which is the same within all the subspaces in the same super-block) matches those of the full matrix of the hamiltonian. In particular, $TS_{114}$ and $TS_{57}$ have the same energy which is equal to the ground state energy of the full-form matrix. We have also noticed that the $TS_{96}$ was the closest to the ground state energy of the QPM after the $TS_{57}$ and the $TS_{114}$.
Therefore, we suspect that the degeneracy of the ground state of $H_{QPM}$ may be due to the presence of these TS.. We have observed that the $TS_{57}$ and the $TS_{114}$ subspaces had a maximum of 8 diamonds, while the $TS_{96}$ subspaces had 6, the 18 state 4, the 2-state 2. These results are summarized in Tab. 4.1

- **108-site:** Although we were not able to calculate the full Hilbert space for this cluster size, we have been able to calculate the dimension of the topological sector consisting in the fully down or the fully up and the mixed up and down (see Sec. 4.2.2 for more details about the sectors on N=108). The former had 7311 states and the latter had the triple, i.e 21933 states. The fully up TS in the 192-site-cluster had a dimension $\geq 200\,000$.

| | | | | | |
|---|---|---|---|---|---|
| N | states(sectors) | 1 | 3(8) | | |
| 12 | $E_{GS}$/site | 0 | -0.333 | | |
| N | states(sectors) | 1 | 21(8) | | |
| 36 | $E_{GS}$/site | 0 | -0.222 | | |
| N | states(sectors) | $TS_1$: 1 | $TS_{57}$: 57(8) | $TS_{114}$: 114(12) | |
| 48 | $E_{GS}$/site | 0 | -0.21702 | -0.21702 | |
| | | $TS_{96}$: 96(12) | $TS_{18}$: 18(24) | $TS_2$: 2(96) | |
| | $E_{GS}$/site | -0.197169 | -0.125 | -0.04167 | |

Table 4.1: Subspaces and "super-blocks" of the 12-site, 36-site and the 48-site cluster. $\frac{V}{t} = -1$. The ground state energy of $TS_{57}$ and of $TS_{114}$ correspond to those of the full-size matrix.

By investigating the fully flippable configurations in each sector ( i.e the $TS_{57}$ and $TS_{114}$), we have observed that the configurations are either "shifted" from one to another or they are composed by different combinations of up/down diamonds. Although we will give a proof of this later on, let us admit for the

moment that the diamond flip in our effective hamiltonian cannot sweep all the translated configurations or transform an up diamond to a down diamond.

At first we can be interested in a way to distinguish one super-block from another which has two different ground state energies, or in TS language, in finding a conserved and unique quantity for each of them. There is one such number which is a clue: the maximum number of diamonds in each sector, that is:

$$N_{d,\alpha} = \max_{i \in TS_\alpha} (n_d(i))$$

where $n_d(i)$ is the number of diamonds in configuration $|i\rangle$.

The maximum number of diamonds could be a possible characterization of the topological *super-blocks* having distinct energies, if we could predict this number without finding it in a brute-force manner (i.e successive applications of H on a random configuration and remembering the maximum number of diamonds throughout the process).

Let us now try to find some numbers that characterize each TS independently in the following chapter:

### 4.1.1 Cut-lines and Plaquette Numbers as Conserved Numbers

We present here two quantities that are conserved in our QPM. Both are by definition of the hamiltonian, conserved within a subspace, which explains our choice since we are looking for invariants of H:

- In a similar way that in [10] we have computed **the number of plaquettes intersected by lines (or *cut-lines*)**: called $\mathbf{N^i_{CT}(i)}$ where $j$ is the direction of the cut-line, as shown on Fig.4.1.
  In fact one might convince oneself with a simple drawing that the $N^j_{CT}(i)$ remain unchanged by the kinetic term of $H$.
  The cut-line values $N^j_{CT}$ are cyclically conserved within a super-block, and the number of possible and distinct permutations for each cut-line gives a lower bound to the size of the super-block. To get a full understanding of the preceding proposition, we invite the reader to observe Tab.4.2 which for example contains the three cut-lines of the $TS_{57}$.

- **The number of different types of plaquettes** each configuration has: $\mathbf{N_p(i)}$. We have noticed that the number of plaquettes $N_p$ is cyclically conserved within a super-block, but unfortunately, they are not sufficient to uniquely describe a super-block as one or more of them have the same plaquette type combinations. The flip term conserves the number of different plaquette types since it transforms a diamond into a diamond.

| Cut-line | I | II | III | IV |
|---|---|---|---|---|
| $H$ | 6 | 2 | 6 | 2 |
| $V_{\frac{2\pi}{3}}$ | 2 | 6 | 2 | 6 |
| $V_{\frac{4\pi}{3}}$ | 6 | 2 | 6 | 2 |
| $H$ | 6 | 2 | 6 | 2 |
| $V_{\frac{2\pi}{3}}$ | 2 | 6 | 2 | 6 |
| $V_{\frac{4\pi}{3}}$ | 2 | 6 | 2 | 6 |
| $H$ | 2 | 6 | 2 | 6 |
| $V_{\frac{2\pi}{3}}$ | 2 | 6 | 2 | 6 |
| $V_{\frac{4\pi}{3}}$ | 6 | 2 | 6 | 2 |
| $H$ | 6 | 2 | 6 | 2 |
| $V_{\frac{2\pi}{3}}$ | 6 | 2 | 6 | 2 |
| $V_{\frac{4\pi}{3}}$ | 2 | 6 | 2 | 6 |
| $H$ | 6 | 2 | 6 | 2 |
| $V_{\frac{2\pi}{3}}$ | 6 | 2 | 6 | 2 |
| $V_{\frac{4\pi}{3}}$ | 6 | 2 | 6 | 2 |
| $H$ | 2 | 6 | 2 | 6 |
| $V_{\frac{2\pi}{3}}$ | 6 | 2 | 6 | 2 |
| $V_{\frac{4\pi}{3}}$ | 6 | 2 | 6 | 2 |
| $H$ | 2 | 6 | 2 | 6 |
| $V_{\frac{2\pi}{3}}$ | 2 | 6 | 2 | 6 |
| $V_{\frac{4\pi}{3}}$ | 2 | 6 | 2 | 6 |
| $H$ | 2 | 6 | 2 | 6 |
| $V_{\frac{2\pi}{3}}$ | 6 | 2 | 6 | 2 |
| $V_{\frac{4\pi}{3}}$ | 2 | 6 | 2 | 6 |

Table 4.2: Cyclically conserved cut-lines of $TS_{57}$. The number of distinct permutations of '6 2' for each cut-line gives the size of the TS, which is 8. We have observed that this is only a lower bound for other TS. $H$,$V_{\frac{2\pi}{3}}$ and $V_{\frac{4\pi}{3}}$ are respectively the black, red and green cut-lines as seen on Fig. 4.1.

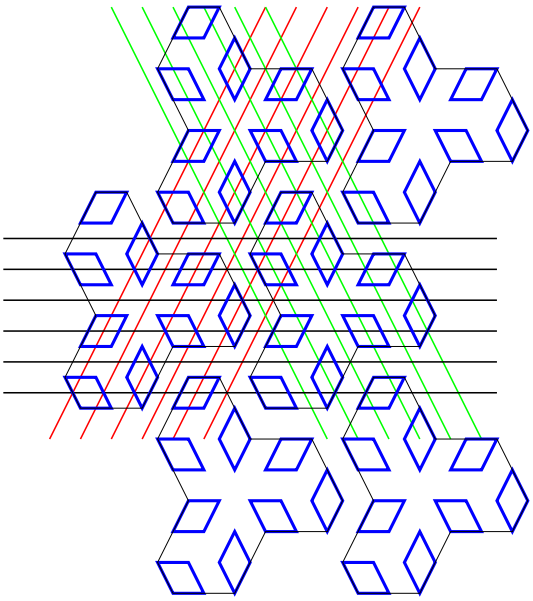

Figure 4.1: Cut-lines in the three directions

## 4.2 Degeneracy of the Ground State and the Fully Flippable States

As we have seen above, the ground state is 8-fold degenerate on the 12-site and on the 36-site lattices. On the other hand the 48-site is 20-fold degenerate. We would now like to understand why we have such numbers and to predict them on larger lattices.

Let us start our argument with the simple case of the 12-site lattice having the fully flippable configuration as depicted on Fig. 4.2. This figure shows configurations of each TS of the flippable super-block on the 12-site cluster. One can convince oneself that the hamiltonian is unable to "shift" these diamonds by one step. Therefore there are 4 different shifted positions and each gives a TS (or a block in the super-block). Reflexion on a horizontal axis gives us the opposite diamond therefore the 8-fold degeneracy is found. We have noticed that this 4-fold degeneracy due to the shift is valid for every maximally flippable states of all types of clusters whose number of sites is a multiple of 12 (each diamond occupies 12 sites).

### 4.2.1 Translations and Sub-lattices

To prove the last statement, let us give a more formal explanation. We have noticed by numeric calculation that the states in $TS_{57}$ and in $TS_{114}$ are invariant by two-step translations in each direction. More explicitly, one can take a unit cell as depicted in Fig.4.3 and translate its plaquettes by two steps in either direction and see that the resulting configuration can be obtained by successive

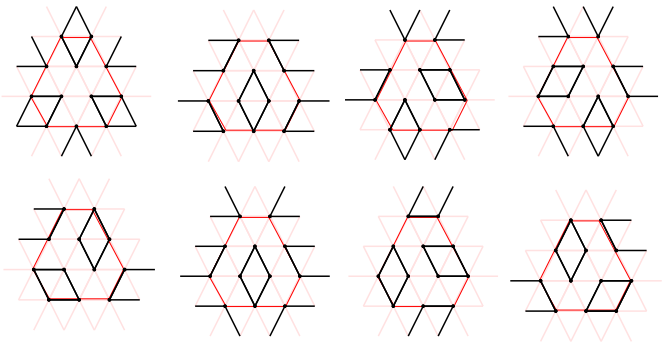

Figure 4.2: Configurations of the 12-site lattice lying on different TS. The upper ones having the "up diamond" are shifted from each other. The lower ones have "down diamonds" and are also shifted from each other. One may convince oneself that these are the only possible shifts that give different configurations.

flips. Formally: let $T_k^2$ be a two step translation in the direction k. Then:

$$T_k^2|\psi_j\rangle = |\psi_j\rangle \quad \forall k$$

where $|\psi_j\rangle = \sum_{i \in TS_j} |i\rangle$ is an equally weighted linear combination of the states in the $TS_j$. In other words, $T^2$ commutes with $H$. On a planar graph, $T^2$ divides the cluster into 4 different parts: each of them are sets of sites that can be connected after a finite number of $T_k^2$ translations. Our idea is to divide the lattice into 4 sub-lattices that we represent by four different colors, for instance: red, green, blue and black. This explains the 4-fold degeneracy of each similar TS since we can permute 4 times the colors to get different combinations. This will be true for all fully flippable configurations $\forall N$ since it is true for any unit cell having up or down diamonds. Furthermore, we will see in the correlations section 5.3 that some of the predictions that follow these facts are confirmed. See Fig. 4.3.

### 4.2.2 Classification of the Fully Flippable States

We now have nearly all the information to explain the degeneracy of the fully flippable configurations in the 48-site cluster. As we have mentioned before, one particularity of this cluster (and of course for all those having N>48) is that it is possible to mix up and down diamonds, but not in a totally free manner if we want close-packed states. The argument is purely topological: they may only organize themselves as lines of up and down diamonds in either 3 directions. Therefore, the law is simple: the degeneracy is equal to the number of ways we may compose these lines of diamonds. As an example, there are 5 possibilities for the 48-site lattice. Applying the 4 "color-permutations" as described earlier, we find 20, which was the degeneracy of the 48-site lattice. See Fig. 4.2. The fully up lines and the fully down lines are invariant under $\frac{2\pi}{3}$ angle rotations, i.e $R_{\frac{2\pi}{3}} \sum_{i \in TS_i} |i\rangle = \sum_{i \in TS_i} |i\rangle$ where the $i$ is restricted to the TS being fully up or fully down.

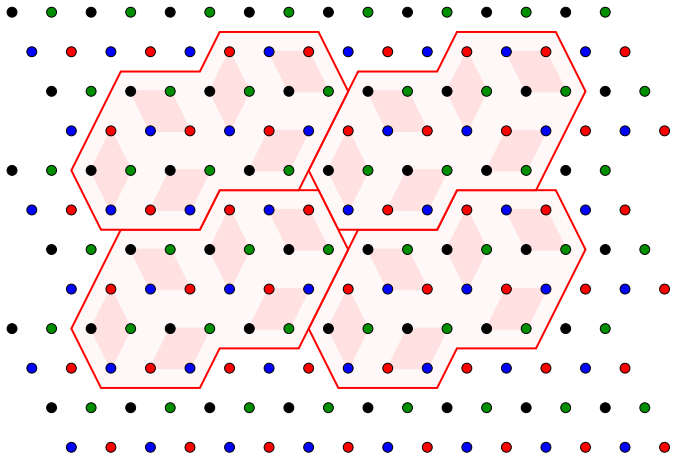

Figure 4.3: Four sub-lattices of the triangular lattice defined by 2 step translations in each direction.

For arbitrary N, the degeneracy of the ground state requires the solution of the following problem: finding the number of circular permutations of 2 objects on a N-site circle, with repetition of the objects. Unfortunately, this problem has no general solution and it must be calculated by hand or by algorithm.

Let us call the solution of the preceding problem $M$. Then by multiplying the $(M-2)$ rotation variant configurations (that is, those which have at least 2 different directions) by 3, the number of rotations, and by adding both rotation-invariant configurations, we get all the sets of lines as seen on Fig. 4.4. Therefore, by taking the 4 different colors into account, we get:

$$4 \cdot ((M-2) \cdot 3 + 2)$$

Where $l$ is the size of a type-A cluster.

| $l$ | N | M | $N_d$ |
|---|---|---|---|
| 2 | 12 | 2 | 8 |
| 4 | 48 | 3 | 20 |
| 6 | 108 | 4 | 32 |
| 8 | 192 | 6 | 56 |
| 10 | 300 | 8 | 80 |

Table 4.3: Expected degeneracy of the ground state on type-A clusters for various N

This rule was confirmed by the exactly solved 48-site cluster. At this point, not only we have the degeneracy of the ground state in hand, but knowing the nature of the situation, we can build configurations in all ground state TS for an arbitrarily large cluster, which will prove to be helpful for the GFMC. We will adopt a more practical notation for this classification, a string of $u, d, r, t$ characters will uniquely classify them, where $u$ is an up diamond, $d$ a down

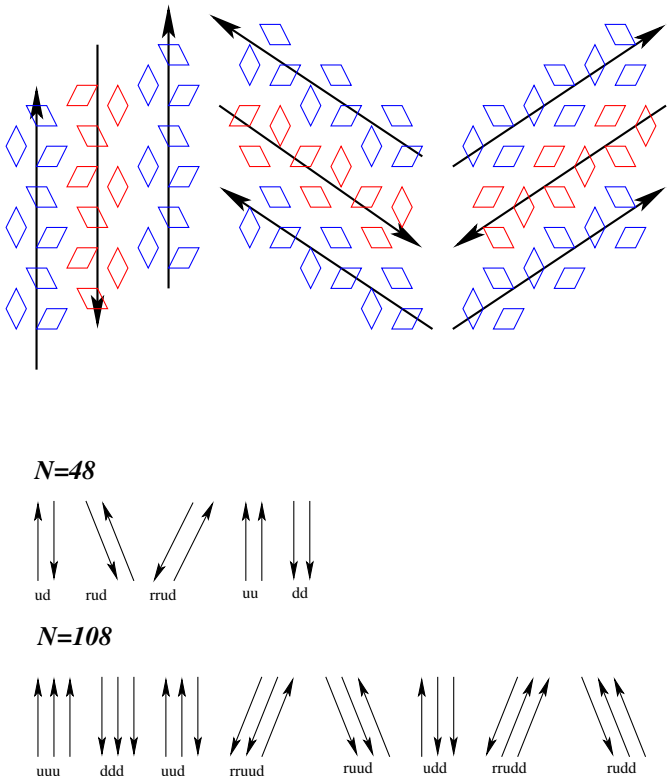


Figure 4.4: In this figure we have represented the diamonds of the 48-site and the 108-site lattices in a special manner: when a line goes upwards, it is a line of up diamonds, whereas a downward line depicts a line of down diamonds. One may notice that rotating the fully up or fully down diamonds has no effect: the new states will be in the same TS. Therefore the ground state degeneracy of the 108-site cluster is $8 \cdot 4 = 32$.

one, $r$ a $R_{\frac{2\pi}{3}}$ rotation and $t$ one of the one-step translations which permutes the colors. Some examples are presented on 4.4.

## 4.3 Topological Gap

If we can find other topological sectors for which ground state energy is the closest to the ground state one of the full hamiltonian, and if we are able to prove it, then we will be able to calculate the topological gap between these TS and those presented in the preceding sections (i.e the fully flippables) and make some conclusions. Here are some possible scenarios for the topological gap:

- The gap may close at a boundary parameter $\frac{V}{t}$ in the thermodynamic limit. This will be a possible phase transition. Suddenly the ground state will be generated by different types of configurations. This is the case of the dimer model on a triangular lattice. It is believed that it has a phase transition around $\frac{V}{t} \cong 0.7$, where the SR RVB-liquid phase becomes a

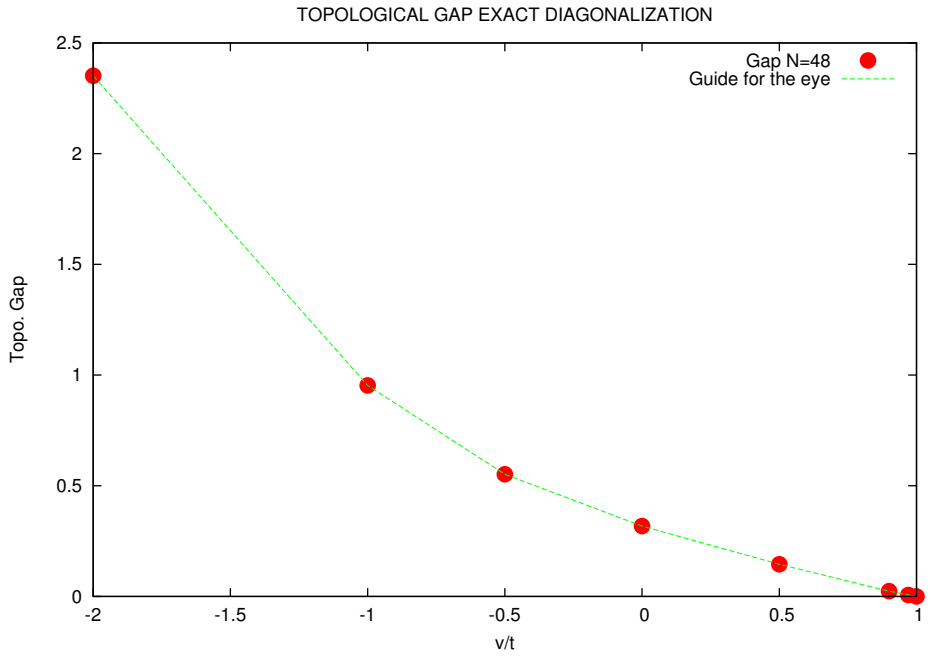


Figure 4.5: Total topological gap $|\Delta_{TG}|$ by exact diagonalization. The green line is a guide for the eye.

$\sqrt{12} \times \sqrt{12}$ phase (from high $\frac{V}{t}$ to low).

- The gap never closes for $\frac{V}{t} < 1$ in the thermodynamic limit. The system is said to be topologically gapped and this is the case of the dimer model on a square lattice. The gap closes at the RK point where all the TS have the same ground state energy.

In any case, this is possible in exact diagonalization since we have the entire Hilbert space. Therefore we have first calculated the topological gap between $TS_{57}$ (or equally $TS_{114}$) and $TS_{96}$:

$$|\Delta_{TG}E| = |E_{TS_{57}} - E_{TS_{96}}|$$

For $\frac{V}{t}$ varying from -1 to 1, the results are shown on Fig.4.5. We see that for N=48, the gap closes at $\frac{V}{t} = 1$, as one would expect since in the RK point, all TS are degenerate. At this point no conclusion can be taken but this is a reference for the GFMC method, where we will calculate this gap for larger N (up to 588) to see the behaviour of the topological gap near the thermodynamic limit.

### 4.3.1 First excited Topological Gaps

Although we have a full knowledge of the $N = 48$ case, how will we produce states in the first excited TS, i.e the equivalent of $TS_{96}$ for larger N? Since the GFMC can only handle a certain number of states at a time and that we do not

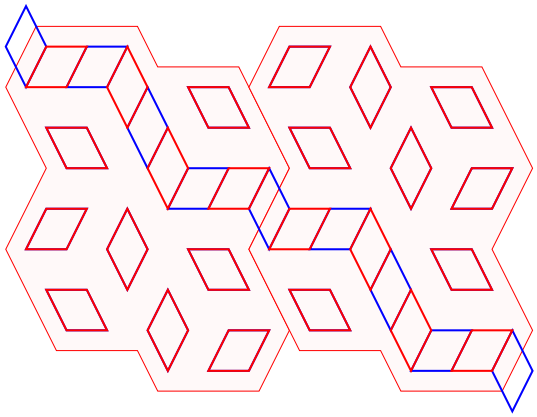

Figure 4.6: Transition graph between a fully flippable state of $ud$ sector and $TS_{96}$. It is understood the plaquette shift replaces the red plaquettes by the blue ones which connected to them. The resulting state has 2 less diamonds

have access to the full Hilbert space (See Appendix A), we must find a general way to create them.

The main property of $TS_{96}$ is the fact that the maximum number of diamonds of the TS, $N_{d,TS_{96}}$, is equal to 6. By comparing the latter with $TS_{114}$ we find that a 1-to-1 operation links the subspaces (a quick look to Tab. 4.1 reminds us that both have the same number of blocks, which is 12): the operation is a *plaquette shift* in a direction that is non-parallel to the line of diamonds, see Fig. 4.6. This operation destroys a diamond each time a boundary between an up diamond and a down diamond is crossed. Therefore, considering a $ud...d$ fully flippable state, we can get states having $N_d = \frac{2 \cdot N}{12} - 2$ which is the only possible value below $\frac{2 \cdot N}{12}$ for a close-packed covering. This proposition is confirmed for $N$ up to $N = 588$, on which the created configurations had in fact 96 diamonds, out of the possible 98 diamonds. Therefore we can be nearly sure that the new sector will be the first excited TS $\forall N$. Note that a plaquette shift in a direction *parallel* to the diamonds relates $TS_{57}$ to $TS_{114}$ for the $N = 48$ lattice, (and all the different TS that have different combinations of up and down diamonds for $N > 48$). One particularity of the shift is that its transition graph has loops around the torus, as in [11].

## 4.4 Plaquette-plaquette Correlations in the Ground State.

It is very interesting to calculate the plaquette-plaquette correlations in order to characterize the phases, i.e either they are crystalline (presence of Long Range Order (LRO)) or liquid (no LRO) which are also called SR RVB-liquid states (Short Range Resonating Valence Bond)[11, 13]. The RVB-liquid states are of great interest because they were proposed as the state in which high temperature superconductors are in their superconducting phase. In order to calculate the

correlations, we introduce the plaquette-plaquette correlator $D_i D_j \equiv D_{ij}$.

The $i$ is the *reference plaquette site* which is one of the twelve plaquettes that can be built around a site. The idea is the following: given a plaquette on site i, then there is a contribution if the site $j$ has a plaquette of the same type as the one on $i$. Roughly, if such is the case for many sites, then the correlation will be high, and the cluster will tend to be crystalline. Note the opposite case: if there are very few contributing $D_{ij}$'s, then the other plaquettes will be favoured, giving a "lower than normal" correlation therefore an *anti-correlation* which is also a sign of LRO. Only correlation tending to $\langle D_i \rangle \langle D_j \rangle$ will be liquid-like as we shall see in the following paragraphs.

### 4.4.1 Correlation Matrix

Calculating correlation is extremely simple, one has to calculate each element of the matrix written below, where $|\psi\rangle$ is a normalized linear combination of states.

$$G_{i\,j} = \langle \psi | D_{ij} | \psi \rangle \tag{4.1}$$

where $|\psi\rangle$ is typically the ground state and $D_{ij}$ is the plaquette operator which is equal to 1 if there is a plaquette of the same type on site $i$ and on site $j$ and 0 otherwise. By arbitrarily choosing the reference $i$, in the absence of LRO, the correlation function should decay with increasing distance $|\mathbf{x_i} - \mathbf{x_j}|$. If the phase is crystalline, then we will find an oscillating correlation corresponding to its structure.

Once this matrix has been calculated, we can either set the reference and choose a direction to get a graph of the decay, or we can graphically represent the correlations on a cluster. Although the former is the most precise, a graphical representation is qualitatively satisfying.

In exact diagonalization we have calculated these correlations on a ground state of the full hamiltonian and on the ground state of different TS. To our surprise, at no $\frac{V}{t}$ do the oscillations decay if we restrict ourselves to some TS, therefore we suspect that the QPM exhibits some LRO at the RK point. However, this is due to the restricted number of states in the TS, in which all sites cannot have all types of plaquettes on each site and due to the finite-size effects. See Sec. 5.3. We shall see that for large N some TS exhibit LRO, others not. Some correlations in function of distance calculated by exact diagonalization have been presented on Fig. 4.7.

We now have reference values to validate our results with a more powerful method: the Green's Function Monte Carlo (GFMC), which will be able to calculate the ground state energies and correlations of much larger systems.

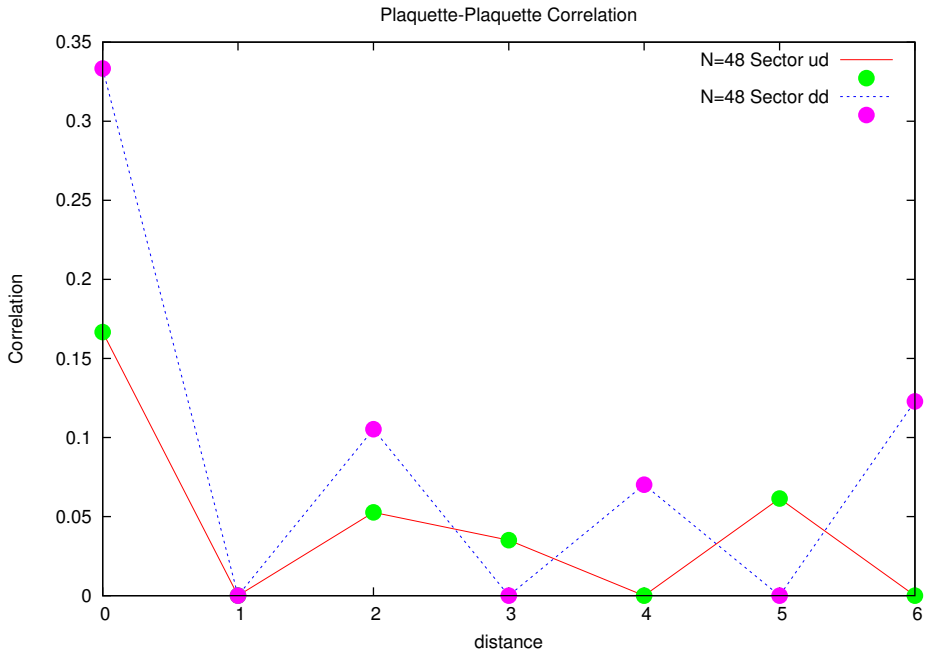


Figure 4.7: Plaquette-Plaquette Correlations for ground states in various TS

# Chapter 5

# Numerical Results Using GFMC

## 5.1 Ground state energy

All the fully flippable TS in the N=48 cluster were rigorously degenerate. However, since we are going to calculate correlations in these sectors for larger N with GFMC in the next sections, we would like to be sure that all the different fully flippable TS described in Sec. 4.2.2 are indeed degenerate in the thermodynamic limit. Results using GFMC show that this is true for all TS up to $N = 432$. The convergence graphs on Fig. 5.2 are examples of the gaps between the two sectors for which correlations are calculated in the following paragraphs.

## 5.2 Topological Gap in the Thermodynamic Limit

In the way described in Sec. 4.3.1, we have generated states in excited TS and ground state TS for N ranging from 48 to 588 in order to estimate the gap in thermodynamic limit by size-scaling. Results are shown on Fig. 5.2. On the x axis we have $\frac{1}{\sqrt{N}}$ and the total energy gap on the y axis. Thermodynamic limit is towards the left.

One can see that the gap never closes $\forall \frac{V}{t} < 1$ at the thermodynamic limit. This was not very surprising since in exact diagonalization, we had found that the first excitation had lower energy than the ground state of our purposed excited TS, that is $TS_{96}$ for the 48-site case. First excitations are more likely to be perturbations of the configurations within the fully flippable topological sectors.

## 5.3 Static Correlations

Since there is probably no phase transition before the vicinity of RK point, we are probably in a case similar to the QDM on a square lattice[12].
Instead of the correlation matrix eq.(4.1) in Sec. 4.4, we will use the general correlation defined in [12], which is the following:

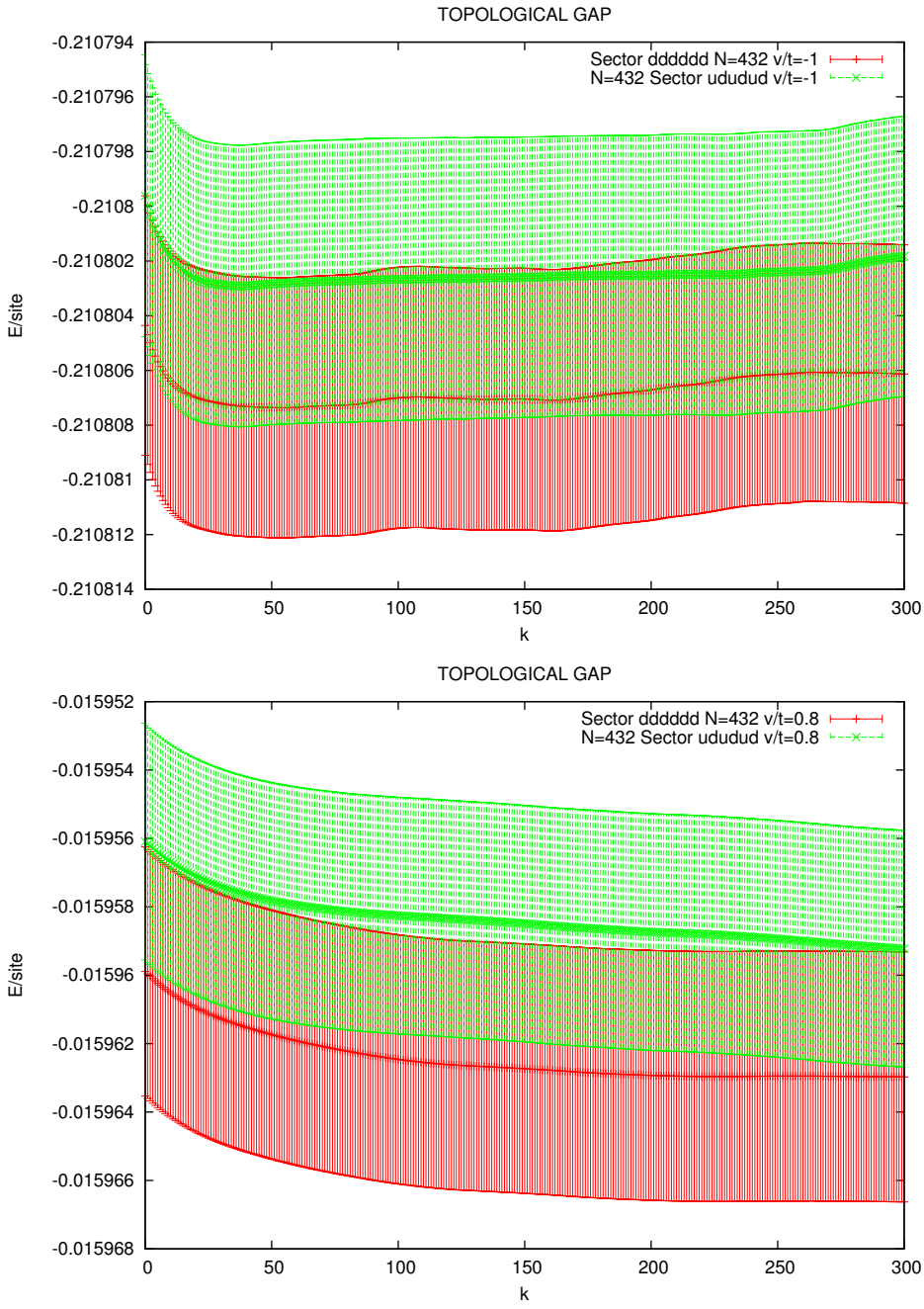


Figure 5.1: Topological gap between two different fully flippable TS. $\frac{V}{t} = -1$(above), $\frac{V}{t} = 0.8$ (bottom).

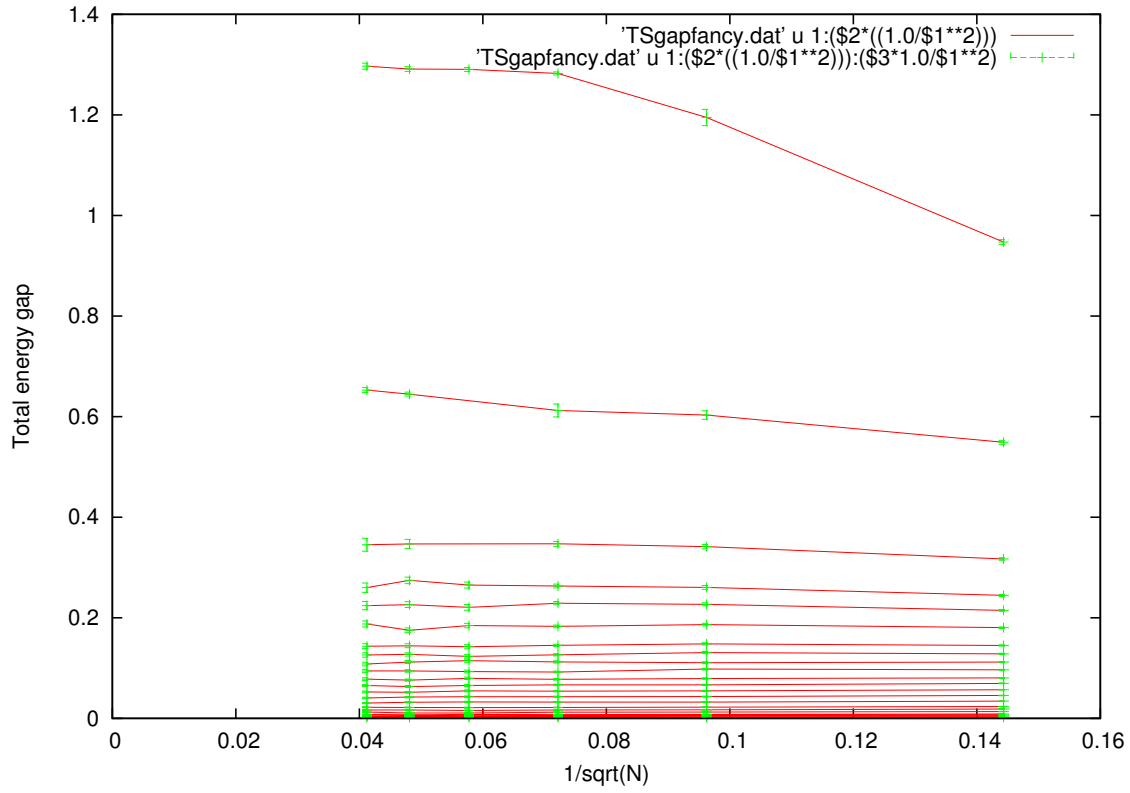


Figure 5.2: Topological gap towards the thermodynamic limit, for $\frac{V}{t}$ varied from -1 (top) to 1 (bottom)

$$C_{(i\,j)(k\,l)} = \frac{\langle\psi|D_iD_j|\psi\rangle - \langle\psi|D_i|\psi\rangle\langle\psi|D_j|\psi\rangle}{\sqrt{\langle\psi|D_i^2|\psi\rangle - \langle\psi|D_i|\psi\rangle}\sqrt{\langle\psi|D_j^2|\psi\rangle - \langle\psi|D_j|\psi\rangle}} \tag{5.1}$$

where $D_i$ is defined as the same way as in Sec.4.4. Since it is either 0 or 1, $D_i^2 = D_i$. Therefore with $G_{i\,j}$ as defined in eq.(4.1), (5.1) becomes:

$$C_{(i\,j)(k\,l)} = \frac{G_{i\,j} - \langle D_i\rangle_\psi\langle D_j\rangle_\psi}{\sqrt{(\langle D_i\rangle_\psi - \langle D_i\rangle_\psi^2)\cdot(\langle D_j\rangle_\psi - \langle D_j\rangle_\psi^2)}}$$

This definition will be more appropriate to compare the correlations of different TS. In fact, in contrast to the dimer liquid, $\exists j\,|\langle D_i\rangle_\psi \neq \langle D_j\rangle_\psi$. Furthermore, in contrast to what one might expect because there are exactly 12 types of plaquettes that can be built around one site:

$$\langle D_i\rangle_\psi \neq \frac{1}{12} \tag{5.2}$$

if $|\psi>$is a state (or a linear combination of states) in one TS.

| 48 | $uu$ | $ud$ | $dd$ | | |
|---|---|---|---|---|---|
| $< D_i >$ | $\frac{1}{3}$ | $\frac{1}{6}, \frac{1}{3}$ | $\frac{1}{3}$ | | |
| 108 | $uuu$ | $uud$ | $udd$ | $ddd$ | |
| $< D_i >$ | $\frac{1}{3}$ | $\frac{1}{9}, \frac{2}{9}, \frac{1}{3}$ | $\frac{1}{9}, \frac{2}{9}, \frac{1}{3}$ | $\frac{1}{3}$ | |
| 192 | $uuuu$ | $uuud$ | $uudd$ | $uddd$ | $udud$ |
| $< D_i >$ | $\frac{1}{3}$ | $\frac{1}{4}, \frac{1}{3}, \frac{1}{12}$ | $\frac{1}{6}, \frac{1}{3}$ | $\frac{1}{4}, \frac{1}{3}, \frac{1}{12}$ | $\frac{1}{6}, \frac{1}{3}$ |
| 300 | $uuuud$ | $uuudd$ | $uuddd$ | $udddd$ | $uuuuu$ |
| $< D_i >$ | $\frac{1}{3}, \frac{4}{15}, \frac{1}{15}$ | $\frac{1}{5}, \frac{1}{3}, \frac{2}{15}$ | $\frac{2}{15}, \frac{1}{3}, \frac{1}{5}$ | $\frac{1}{3}, \frac{4}{15}, \frac{1}{15}$ | $\frac{1}{3}$ |

Table 5.1: Different possibilities of $< D_i >$ for N=48,108,192,300

As a test, however, we have checked that the preceding mean value eq. 5.2 on an equally weighted linear combination of all the ground states of all TS, that is $|\psi\rangle = \frac{1}{N}\sum_{i\in TS_i} |c_{GS_i}\rangle$, with $N$ the number of states, does in fact tend to $\frac{1}{12}$.

The reason of eq.(5.2) comes from the breaking of the translational invariance as described in Sec. 4.2.1. To overcome this problem, the defined sub-lattices in the same section will be of great help: by counting the number of different plaquettes on each color in a unit cell, one gets $\langle D_i \rangle_\psi$.

More explicitly, let us call the previous number $N_c^p$ where $c$ sets the sub-lattice color, and $p$ the plaquette type. The total number of sites enclosed in the unit cell for each sub-lattice is $3 \cdot \frac{l}{2}$, where $l$ was defined in Sec. 4.2.2. Therefore:

$$\langle D_i^p \rangle = \frac{N_c^p}{3 \cdot \frac{l}{2}}$$

if site $i$ is of color c. It is understood that $D_i^p$ is the plaquette operator which concerns only the plaquette of type $p$. All up diamonds will share the same plaquette types on each color, and all down diamonds will share three other plaquettes types on the same color, and only one will be in common. Therefore, we can find the different $\langle D_i^p \rangle$ for each $N$ in a certain fully flippable TS, and some examples are listed in Tab. 5.1.

### 5.3.1 Results of Static Plaquette-plaquette Correlations Using GFMC

We have calculated the correlations on many sectors and we will present some of them here: the fully down TS and the equally mixed *udud...udud* sector. This choice comes from the fact that we can compare the correlation for many different N and eventually observe the finite-size effects, which obviously disappears for $N \geq 192$. In the following, we have used the correlation defined in the section above and we underline the fact that the $< D_i >$ terms were always one of those which had been predicted in the same way as in Tab. 5.1.

Results of the correlations in GFMC for $N = 192, 300, 432, 588$ on sector fully down $d...d$ at the RK point are shown on Fig. 5.3 and on Fig. 5.4 in a log log scale. The fit concerns the N=588 results and exhibits a power law decay of the envelope (since only values $x > 0$, $y > 0$ are plotted on a log-log figure). The 48 site correlation comes from exact diagonalization. The decay in this TS is similar to what we expected, that is, the transition is critical therefore the correlations decay as a power law. However, this is not always the case as we shall see.
Results for the $udud...udud$ sector can only be calculated for sectors having an $\frac{l}{2}$ which is a multiple of 2. Therefore we have presented the correlations for $N = 192, 432$ at the RK point on Fig. 5.5.

To our surprise, the correlations do not decay at the RK point for any other TS than the fully up or the fully down. Fig. 5.5 shows that the correlation oscillates around the predicted averages $\langle D_i \rangle \langle D_j \rangle$: the phase tends to be very crystalline since if there is a certain plaquette on the reference site, there are peaks at different distances which are close to 20% and they do not seem to decay even for large N, very far from the reference plaquette.

The trend is that the more the sectors become mixed with up and down diamonds, the more the model exhibits plaquette-plaquette LRO. This fact can be seen on Fig. 5.6 where we have presented some variously up and down mixed sectors.

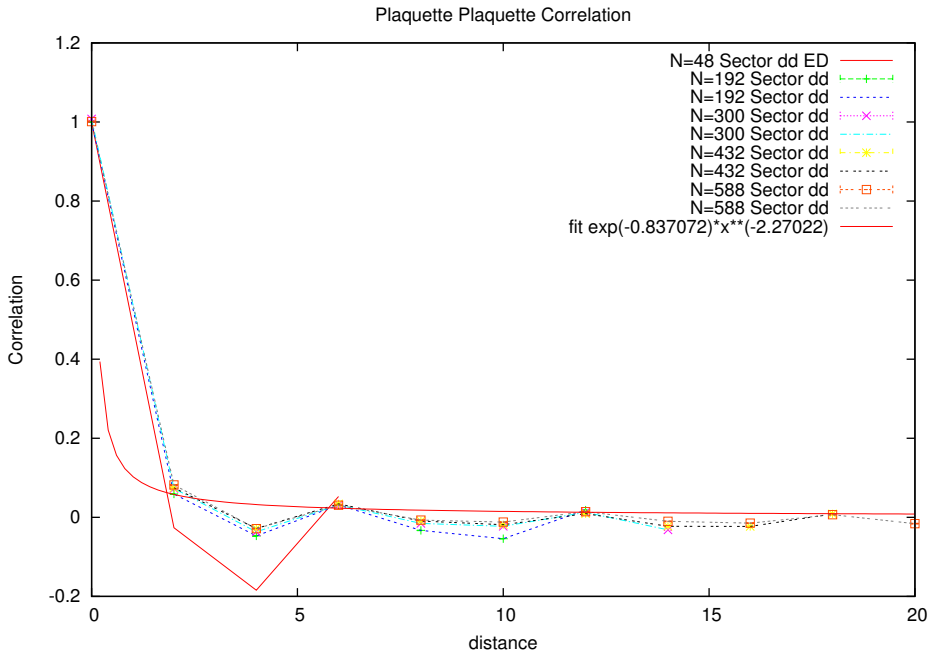


Figure 5.3: Correlation for various N, Sector dddd

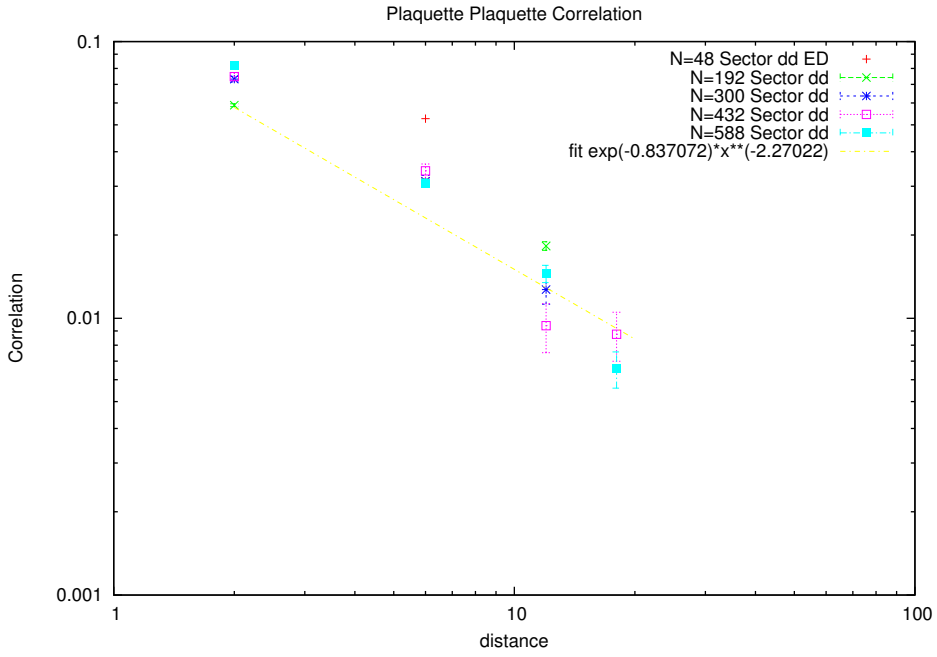


Figure 5.4: Correlation for various N, Sector dddd... . The lower figure is in a log log scale.

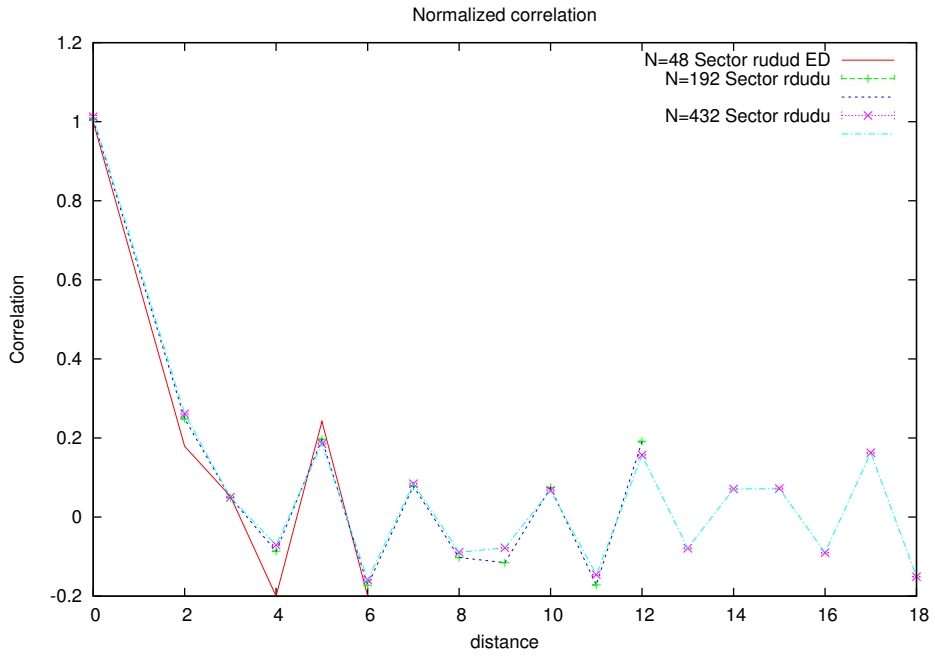


Figure 5.5: Correlation for various N, sector udud...

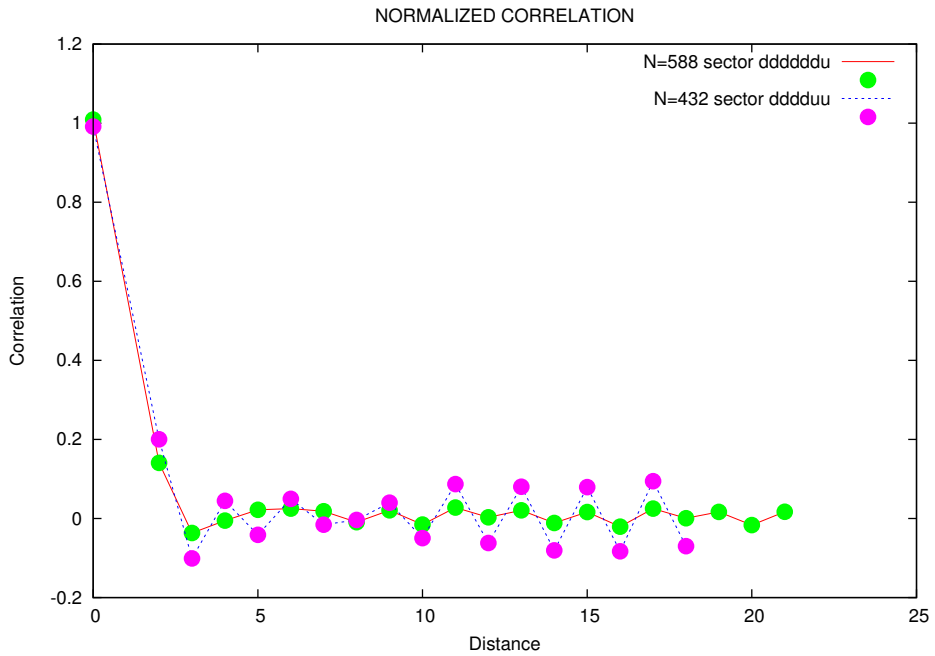


Figure 5.6: Correlations on various sectors for N=432, 588. Note the way the order gets more and more crystalline when we mix up and down lines of diamonds. (green points vs purple points)

# Chapter 6

# Conclusion and Outlook

In this diploma we have studied a Quantum Plaquette Model which is an effective model of the SU(4) invariant hamiltonian having spin and orbital degrees of freedom. Proceeding with exact diagonalizations, we have found that the ground state is 20-fold degenerate on the 48-site cluster. Then we have calculated the number of different topological sectors (TS) for this case. We found that there were in total 452 TS from which 152 of them had two or more states (i.e non-staggered) and 20 of them had their ground state energy equal to the ground state energy of the effective hamiltonian. We observed that the configurations in these sectors were the fully flippable ones, this permitted us to find a rule to count and to build them for an arbitrary N. It would have been interesting to confirm this rule by calculating the spectrum of the 108-site lattice. However, an extrapolation from our values for the 12, 48 site clusters show that the dimension of the hilbert space would be in the order of $10^7$. Furthermore, some numerical calculations showed that the fully up or down sub-hilbert space was of dimension 7311 for $N = 108$ and $> 2 \cdot 10^5$ for the $N = 192$ case.

On the other hand the first excited TS in the 48-site cluster is easy to obtain from these fully flippable sectors and we were able to build them for various clusters.

Having this information in hand, we were able to generate configurations for an arbitrary N for use with the Green's Function Monte Carlo algorithm (GFMC), which has permitted us to calculate the ground state energy (therefore topological gaps) and static plaquette-plaquette correlations on clusters up to $N = 588$ on the fully flippable TS. They showed us that the topological gap between the first excited TS and the fully flippable TS never closes at the thermodynamic limit $\forall \frac{V}{t} < 1$ and that the correlations at $\frac{V}{t} = 1$ decay as a power law only on the fully up of the fully down TS, whereas correlations on mixed up and down sectors exhibited LRO.

A good characterization of all the topological sectors, and not only the fully flippable ones may be interesting because if we could find such a classification, we would be able to calculate plaquette-plaquette correlations on topological sectors different than the fully flippable ones on the GFMC, and observe if they are either RVB-liquid like or not at the RK point. Our characterizations with cut-lines and sub-lattices (not written in this report) were not enough to

uniquely classify them, but perhaps the combination of the two may give a unique classification of all TS.

Of course, the next steps would be to understand why the correlations decay on certain TS and not on others at the RK point, their structure and the physical consequences of such a behaviour. It will also be interesting to underline the critical behaviour of the transition by calculating plaquette-plaquette correlations below the RK point, or correlations on ground states mixed within different TS. Unfortunately, the latter requires to completely review the reconfiguration process in the GFMC (see the branching in the appendix) which favours only one TS after a large number of iterations.

## Acknowledgements

I would like to thank the interesting conversations with Arnaud Ralko who has devoted a lot of his time to understand this peculiar model, the patience of both J. Dorier and A. Gellé who had accepted me in their office and who have guided me through this research, all those of the "7th floor" of the building who have contributed to its friendly atmosphere and my supervisor F. Mila who always had interesting propositions for my work, his inspiring lessons throughout my studies at the EPFL, and his sympathy in all situations.

# Appendix A

# Basic Principles of the Green's Function Monte Carlo (GFMC) Algorithm

We wish to calculate the ground state of a finite-size quantum plaquette model. Although we have seen in the preceding chapters that the exact diagonalization of the hamiltonian is possible and gives us all eigenvalues and eigenvectors, it quickly becomes impossible to calculate the energy on larger clusters. In this section, we will describe a powerful method that we have used to calculate the ground state energy and the plaquette-plaquette correlations on clusters having up to 588 sites. This method has been studied and implemented by S. Sorella and F. Becca[18, 17, 14], and has been successfully used in the work of *Ralko et al*[10] on the QDM on the triangular lattice. The following sections will be an overview of [18, 17, 14].

## A.1 Power Method

Before seeing the Monte Carlo algorithm itself, let us first explore a theoretical way to filter out the ground state, using the well known *power method*.

Let $|\psi_T\rangle$be a trial state having a non-zero overlap with the ground state, and assume an operator given by $G = \Lambda - H$ where $H$ is the hamiltonian of the system, and $\Lambda = \lambda \mathbf{1}$

Considering a $\lambda$ greater than the highest eigenvalue, the following series converges:

$$|\psi_{n+1}\rangle = G^{n+1}|\psi_T\rangle = \sum_i (\lambda - E_i)^{n+1} \alpha_i |\phi_i\rangle$$

with $|\psi_T\rangle = \sum_i \alpha_i |\phi_i\rangle$ a linear combination of the eigenvectors $\{|\phi_i\rangle\}$. Separating the sum we get:

$$G^n|\psi_T\rangle = (\lambda - E_0)^n \left\{ \alpha_0|\phi_0\rangle + \sum_{i\neq 0} \frac{(\lambda - E_i)^n}{(\lambda - E_0)^n} \alpha_i |\phi_i\rangle \right\}$$

if $\lambda$ is well chosen then the right hand term in the brackets above becomes small compared to $\alpha_0|\phi_0\rangle$ because $(\lambda - E_i)/(\lambda - E_0) < 1$. After many applications of $G$, the trial state becomes:

$$|\psi_n\rangle \equiv G^n|\psi_T\rangle \rightarrow |\psi_{GS}\rangle \equiv (\lambda - E_0)^n \alpha_0|\phi_0\rangle \quad , n \rightarrow \infty$$

Thus we have filtered out the ground state. One big problem is that applications of $G$ on a state generates as many states as $G$ has off-diagonal terms on a line, which generate other states and so on, easily exceeding the memory of a computer. Therefore, exact diagonalization methods quickly overwhelm the capacities of the computer. That is why we wish to make this calculation stochastically, and we will present the Green's Function Monte Carlo method in the following paragraphs.

## A.2 Calculation with Walkers

Let (x,w) be a *walker*. That is, a state x (a certain configuration of plaquettes/dimers/spins) and a weight associated to this state. Walkers -as their name suggest- will walk the Hilbert space stochastically, following a certain probability scheme given by the dynamics of the system. Let us call the joint probability $P_n(x, w)$ the probability of finding a walker on configuration x with weight $w$ at step $n$. The Monte Carlo process will distribute an initial set of randomly distributed walkers (within the entire Hilbert space or within a certain TS) according to a probability distribution which determines the ground state wave function after a large number of iterations. More technically:

$$\psi_n(x) \equiv \langle x|\psi_n\rangle = \int dw\, w \cdot P_n(x, w) \tag{A.1}$$

The montecarlo method as described above will define a Markov process. Now let us get into some definitions: assume a stochastic matrix $p$, whose elements are given by:

$$p_{x'x} = \frac{G_{x'x}}{b_x}$$

where $b_x = \sum_{x'} G_{x'x}$. At each montecarlo step, a new step is chosen among the non-zero elements of a line of the $p_{x'x}$ matrix, and it's new weight is given by:[1]

$$w' = b_x w \tag{A.2}$$

In a few words, a line of the $p$ matrix gives the uniform transition probabilities of a certain walker. The transition itself will be chosen randomly, but as we will see later a guiding function may give higher weights to some transitions, in order to help convergence. As an example, in the RK point the best guiding function is a uniform function, since the ground state will consist in an equally weighted

[1] Although we will see that this is theoretically correct, in order to help the convergence we choose a slightly different coefficient. In our case it is w=wconf(j)*dexp((wsto(j)-lambda)*tleft) $w' = w \cdot \exp((E_{tot} - \lambda) \cdot t)$ where $t$ is the "time left". See the GFMC enhancements.

linear combination of the walkers in the TS. However, for $\frac{V}{t} < 0$, a guiding function that favours fully flippable configurations dramatically improves the convergence.

Now let us define formally a *transition probability* from state $x$ to state $x'$, with the weight evolution as written above:

$$P_{tr}(x, w, n|x', w', n+1) = p_{x'x}\delta(w' - b_x w)$$

The probability of having a walker $(x', w')$ at step (or time step) $n$ is therefore given by all the possibilities of coming to that point, hence:

$$P_{n+1}(x', w') = \sum_x \frac{p_{x'x}}{b_x} P_n(x, w) \tag{A.3}$$

which defines a Markovian process.

*Proof:* if $P_n(x, w)\, dw$ is the probability of having a walker on configuration x with weight $w \in (w, w + dw)$ and if $P_n(x', w')\, dw'$ is defined in the same manner then:

$$\begin{aligned} P_{n+1}(x', w')\, dw' &= \sum_x P_{tr} P_n(x, w)\, dw \\ &= \sum_x p_{x'x}\delta(w' - b_x w)\, P_n(x, w)\, dw \\ &= \sum_x \frac{p_{x'x}}{b_x}\delta(w' - w')\, P_n(x, w)\, dw' \end{aligned}$$

where in the second line, $w$ has been replaced according to eq. (A.2). This calculation yields eq. (A.3) since $\delta(w' - w') = 1$ and by dividing both sides by $dw'$.

Let us now investigate the mean values of the weight variable, or more generally, the moments of that variable. The definition of the moment of the random variable $w$ is given by:

$$M_{1,n+1}(x') = \int dw'\, w' \cdot P_{n+1}(w', x')$$

After $n$ iterations, we find that:

$$M_{1,n+1}(x') = \textstyle\sum_x (G^{n+1})_{x'x} M_{1,0}(x)$$

And it is easy to verify that $M_{1,n}(x') \to \langle x|\psi_0\rangle$, $n \to \infty$

Therefore eq. (A.1) defines the Markovian process given at eq. (A.3) whose first moment yields the ground state. We suppose that the Markov process $P_n(w, x)$ tends to a stationary distribution for $n$ large enough, although this requires some work to demonstrate it [17]. At this state, we have found a stochastic method to filter out the ground state wave function, and the basics of the Green's function Monte Carlo are soon established. We can proceed to the calculation of the ground state energy, as soon as we have introduced the *guiding function* (also called *importance sampling*)

### A.2.1 Guiding Function

In order to help the convergence, we will take a slightly modified operator, $\tilde{G}$ given by:

$$\tilde{G}_{x'x} = \frac{\psi_g(x')}{\psi_g(x)} G_{x',x} \tag{A.4}$$

where the $\psi_G(x)$ is precisely the *guiding wave function*. Under these conditions the local energy is given by:

$$e(x) = \frac{\sum_{x'} \psi_g(x') H_{x',x}}{\psi_g(x)} \tag{A.5}$$

If the guiding function is exactly equal to the ground state wave function $\psi_g(x) = \psi_0(x)$ then $e(x) = E_0$ and the local energy does not depend on $x$. In fact, writing eq. (A.5) in Dirac notation, using completeness of $|x>$ and symmetry of H, we get:

$$\sum_{x'} \frac{\langle \psi_0 | x' \rangle}{\langle x | \psi_0 \rangle} \langle x' | H | x \rangle = \frac{1}{\langle x | \psi_0 \rangle} \langle x | H | \psi_0 \rangle = E_0$$

Therefore we see that a good choice of the guiding function $\psi_g(x)$ will help the convergence. The calculations in the preceding sections are also valid for the new wave function for which the decomposition is given by $\psi_g(x)\phi_i(x)$. In fact, if $|\phi_i\rangle$ is an eigenvector of $H$, then $\psi_g(x)\langle x|\phi_i\rangle$ is also an eigenvector with the same eigenvalue. Hence, with the guiding function eq. (A.1) reads:

$$\tilde{\psi}_n(x) = \psi_g(x)\langle x|\psi_n\rangle = \int dw \, w \cdot P_n(x, w) \tag{A.6}$$

In our case, a good guiding function is:

$$\psi_g(x) = \exp(\beta N_d(x))$$

where $\beta$ is parameter to be chosen according to the parameter of the system, and $N_d(x)$ the number of diamonds on configuration $x$. For instance, far below the RK point a large $\beta$ will favour configurations having a large number of configurations, whereas at the RK point $\beta = 0$ will be an exact solution since the ground state is an equally weighted linear combination of all the configurations of the TS.

## A.3 Energy Calculation

The expectation value of the energy is given by:

$$E(n) = \frac{\langle \psi_g | H | \psi_g \rangle}{\langle \psi_g | \psi_g \rangle} = \frac{\sum_x e(x) \psi_g^2(x)}{\sum_x \psi_g^2(x)}$$

where $e(x)$ is the *local energy* defined by:

$$e(x) = \frac{\langle x|H|\psi_g\rangle}{\langle x|\psi_g\rangle}$$

Therefore, numerically, the energy expectation value can be calculated by averaging the local energy observable, distributed according to $p_e(x)$ defined by:

$$p_e(x) = \frac{\psi_g^2(x)}{\sum_{x'} \psi_g^2(x')}$$

Returning to our original problem, most generally, with the $G$ matrix notation, a biased estimator of the energy is:

$$\begin{aligned} \lambda - E_0 &= \frac{\langle\psi|G|\psi_0\rangle}{\langle\psi|\psi_0\rangle} \\ &= \frac{\sum_{x'\,x}\langle\psi|x'\rangle G_{x'\,x}\langle x|\psi_0\rangle}{\sum_x \langle\psi|x\rangle\langle x|\psi_0\rangle} \end{aligned} \tag{A.7}$$

Inserting the expressions (A.4) and (A.6) we get:

$$\begin{aligned} &= \frac{\sum_{x',x} \psi(x')\frac{\psi_g(x)}{\psi_g(x')}\tilde{G}_{x'\,x}\psi_0(x)}{\sum_x \psi(x)\psi_0(x)} \\ &= \frac{\sum_{x',x} \frac{\psi(x')}{\psi_g(x')}\tilde{G}_{x'\,x}\tilde{\psi}_0(x)}{\sum_x \frac{\psi(x)}{\psi_g(x)}\tilde{\psi}_0(x)} \end{aligned}$$

If we had we chosen $\psi = \psi_g$ , i.e the same as in the definition of $\tilde{G}$, the latter equation would finally read:

$$= \lim_{n\to\infty} \frac{\sum_{x,x'} \tilde{G}_{x,x'} \int dw\, w \cdot P_n(w,x')}{\sum_x \int dw\, w \cdot P_n(w,x)}$$

The local energy becomes (taking $G$ instead of $H$) $e(x) = \sum_x \tilde{G}_{x'x} = b_x$, calculating the energy is equivalent to averaging the local energy $b_x$, weighted by $\int dw\, w \cdot P_n(w,x')$:

$$\lambda - E_0 = \frac{\sum_x b_x \int dw\, w \cdot P_n(w,x')}{\sum_x \int dw\, w \cdot P_n(w,x')} = \frac{\langle b_x w\rangle}{\langle w\rangle}$$

or even

$$E_0 = \frac{\langle(\lambda - b_x)w\rangle}{\langle w\rangle}$$

where by definition, the mean value of an observable $A(x,w)$ is given by

$$\langle A\rangle = \sum_x \int dw\, A(x,w) \cdot P_n(x,w)$$

In our program, the mean values will be calculated in a discrete manner, i.e

$$\langle A(x,w)\rangle = \lim_{n\to\infty} \frac{1}{n}\sum_{i=1}^{n} A(x_i,w_i)$$

At this point, our goal is clear: we must have a set of $w$ and $b_x w$ distributed according to the Markov law of the underlying dynamics, large enough to have good statistics and compute $E_0$. However, some convergence problems will arise due to the weight factors of the walkers. In fact, they will quickly diverge or nullify leading to huge fluctuations of the energy. At a certain large iteration L:

$$w_L = \prod_{i=0}^{L} b_{x_i} w \to \begin{cases} 0 & b<1 \\ \infty & b>1 \end{cases}$$

where the conditions must be understood as a general behaviour of b. Lets try to remedy to this problem. We make the first $n-L$ iterations, where $n-L$ is large enough to have a well distributed set of walkers (i.e see eq. (A.1). Let us now assume that all the weights before $n-L$ are equal to 1. Then we have,

$$w_n^L = \prod_{i=0}^{L} b_{x_{n-i}}$$

Which is then well defined. In this approximation, the energy is given by:

$$\lambda - E_0 = \frac{\sum_n b_{x_n} w_n^L}{\sum_n w_n^L}$$

Unfortunately, the problem remains when L is large because the new weights $w_n^L$ still grow exponentially, since it is a product of either very large of very small factors. Its variance in the energy average may diverge. One way to remedy to this problem is by making each iteration with a large number of walkers and by considering a reconfiguration of the weights called *branching*, where the insignificant walkers are dropped. See the dedicated section below.

At this point, we have the energy of the ground state and our algorithm will theoretically work, however there are still many other enhancements that can be made to improve convergence.

## A.4 Static Correlations calculation

Other local operators may be calculated in the preceding section simply by replacing the local energy by any other diagonal operators $\bar{O}$. The local operator is:

$$O(x) = \frac{\langle x|\bar{O}|\psi_g\rangle}{\langle x|\psi_g\rangle}$$

Taking $O = D_i D_j$ we can calculate the correlations in the ground state. However, in order to reduce the error in the biased estimator in eq. (A.7) we can let the state evolve during a certain time $\tau_{bias}$,

$$\begin{aligned}\langle O\rangle_n &= \frac{\langle\psi_g|e^{H\tau_{bias}}\bar{O}|\psi_n\rangle}{\langle\psi_g|e^{-H\tau_{bias}}|\psi_n\rangle} \\ &= \frac{\sum_m O(x_m)\cdot w_m^L}{\sum_m w_m^L}\end{aligned}$$

before starting to calculate the expectation value of O, since according to the power method $e^{-H\tau}|\psi_g\rangle \to |\psi_0\rangle$, hence the biased estimator is less biased.

## A.5 Enhancements to the GFMC

### A.5.1 Imaginary Time

This step is a purely artificial step. In fact, the probability of having no transition (i.e diagonal element of H) is quite high and our montecarlo would freeze in the same state for a few iterations, losing precious generations. Instead, we can consider the probability of having off-diagonal moves -that is, a flip of plaquettes or diamonds for example- during a certain *imaginary* time $\tau_{bra}$, at each iteration. By this manner, one iteration would cover a larger time than one move per iteration, considerably speeding up the method. A good choice of $\tau_{bra}$ helps convergence.
In practice, this is done in the following way: let $k$ be the number of reconfigurations at each step. The probability of having an off-diagonal move is usually quite low. So let us define the probability of doing $k$ diagonal moves with probability $P_d^k$ (where nothing happens) and one off-diagonal move of probability $(1-P_d)$ by:

$$t(k) = {P_d}^k(1-P_d)$$

Let us write this in terms of imaginary time $\Delta\tau$, which is a continuous variable.

$$\tilde{t}(\Delta\tau) = P_d^{\Delta\tau}(1-P_d)^{\Delta\tau}$$

We consider that past a certain limit $\Delta\tau_{bra}$, $t(\Delta\tau) = 0$. By normalizing it, we get:

$$\tilde{t}(\Delta\tau) = \frac{\log(P_d)}{P_d^{\Delta\tau_{max}} - 1} P_d^{\Delta\tau}$$

Since $P_d^{\Delta\tau_{max}}$ must be small, the denominator is approximated to$-1$. For practical reasons, we wish to generate this distribution with a randomly distributed number $\zeta \in (0,1)$:

$$\tilde{t}(\Delta\tau)d(\Delta\tau) = P(\zeta)d\zeta$$

By integrating from 0 to $\Delta\tau$ we get:

$$\Delta\tau = \frac{\log(1-\zeta)}{\log P_d}$$

And finally, since $P_d$ is close to 1, $\log(1-(1-P_d)) \cong -(1-P_d)$ we get:

$$\Delta\tau \cong \frac{\log(1-\zeta)}{P_d - 1}$$

This is the time taken in an attempt to make an off-diagonal move.

### A.5.2 Branching

After some iterations, the weight of the walker may be insignificant compared to the preceding weights. In a multiple walker formulation, instead of keeping them until the end, we discard the low weighted walkers and multiply the more important ones, while having the same number of walkers at the end of the branching.

This reconfiguration process modifies the joint probability distribution:

$$P_n(x_1, ..., x_m, w_1, ..., w_m) = P_n(x_1, w_1)...P_n(x_m, w_m)$$

but not the statistical averages, where $m$ is the number of simultaneous walkers. As mentioned earlier, this method also avoids that the variance of the energy average diverges.
A practical way to do this is the following: on operation is applied to all walkers. Their weights $w$ become all equal and their states $x$ are chosen amongst the old configurations with a probability proportional to the normalized weight (before the reconfiguration) of $x$. By this way, we drop most of the irrelevant walkers.

### A.5.3 Bin Method for Error Estimation

In GFMC, we calculate over N realizations of the same experience in order to reduce the error due to the autocorrelation of the energy. Hence the local energy is:

$$\bar{e} = \frac{1}{N}\sum_{n=1}^{N} e(x_n) \tag{A.8}$$

where $x_n$ is the sequence of configurations generated by the Markov process. However, because of the branching, these $x_n$ are correlated, therefore the variance of $\bar{e}$ is lower than it's true value. To overcome this problem, we make $k$ partial sums of the sum in (A.8) of length $l_{bin}$ so that each partial sum is an independent random variable.

## A.6 Main Steps of the Algorithm

In this section we will explain some of the concepts of the program which can sometimes be a little different than the theory.

1. At first, we must initialize a set of walkers whose distribution over the Hilbert space and weight must be uniform. These walkers $(x, w)$ can be built in the same way as before, see section 2 to the slight difference that the direction of the plaquette is chosen randomly, in order to initialize

randomly, and once a configuration is found, the initialization starts from the beginning (i.e no going back by recursion). However, this method proves to be inefficient for large clusters ($N$>300), and we will be more interested in restricting ourselves to some TS. The fully flippable and their possible first excited TS are easily generated because of their simple structure. A random number of diamond flips gives a uniform distribution of walkers along the considered TS.

2. There are 2 $N_{site}$-dimensional vectors associated to each walker: the "diagonal part" and the "off-diagonal part". The former consists only in the number of diamonds times V and the latter the number of diamonds on a configuration where a flip is made at, times -t. To reduce calculation time, this table is only locally "updated" at each step and not recalculated from beginning to end.

3. Calculation of the $b_x$ term, or any other local operator

4. Initialization of the *imaginary time*. The probability of having an off-diagonal move is given by $P_{hd}(x) = b_x - V\,N_{diam}$ $(=1 - P_d)$. In our case, for a walker on configuration x, we can choose $t_{try}(x) = \frac{\log(1-\zeta)}{-P_{hd}(x)}$ , with $\zeta \in (0,1)$ a random number. $t_{try}(x)$ which is a positive value since $P_{hd}(x)$ is the sum of a off-diagonal part of $G$. If there are no flippable diamonds, $t_{try} \to \infty$. Otherwise, the more diamonds there are, the shorter the trial time will be.

5. Make as much off-diagonal moves as possible within the time $t_{bra}$ and update the weights. However, the new weight is not given by $w' = b_x w$ but by:

$$w = w\,\exp((w - \lambda) \cdot t)$$

   Where t is either $t_{left}$ or $t_{try}$. Of course, the site in which we make the flip is chosen randomly.

6. Update of the 2 vectors associated to the walkers (average and variance)

7. Branching and calculation of the energy after $l$ steps, as explained above. And the loop starts again as many times as we want to get a good convergence (therefore small error-bars)

# Bibliography


[1] P. W. Anderson, Mater. Res. Bull. **8,** 153 (1973); P. Fazekas and P. W. Anderson, Philos. Mag. **30**, 432 (1974)

[2] G. Misguich, D. Serban, and V. Pasquier, Phys. Rev. Lett. **89,** 137202 (2002)

[3] Y.Q. Li, M. Ma, D.N. Shi, F.C. Zhang, Phys. Rev. Lett. **81**,16 (1998)

[4] F. Mila: Phys. Rev. Lett. **81**,11 (1998)

[5] François Vernay,thesis: *Dégénéresence orbitale et ordre magnétique sur le réseau triangulaire: Le cas des composés $LiNiO_2$ et $NaNiO_2$ (2005)*

[6] M. Mambrini and F. Mila: RVB description of the low-energy singlets of the spin 1/2 kagomé antiferromagnet

[7] B. Bernu, P. Lecheminant, C. Lhuiller, L. Pierre, Phys. Rev. B **50,** 10048

[8] K. Penc, P. Fazekas, and F. Mila: Plaquette phases in SU(4) models

[9] R. Moessner, S. L. Sondhi, Phys. Rev. Lett. **86,** 1881 (2001)

[10] A. Ralko, M. Ferrero, F. Becca, D. Ivanov, and F. Mila, Phys. Rev. B, **71,** 224109 (2005)

[11] D. S. Rokhsar, S. A. Kivelson, Phys. Rev. Lett. **61,** 20 (1988)

[12] P. W. Leung, K. C. Chui, K. J. Runge, Phys. Rev. B **54,**18 (1996)

[13] P. Fendley, R. Moessner, S.L. Sondhi, Phys. Rev. B **66,** 214513 (2002)

[14] Matteo Calandra Buonaura, S. Sorella, Phys. Rev. B**, 57,**18 (1998)

[15] M. van den Bossche, F.-C. Zhang, R. Mila, Eur. Phys J. B. **17**, 367-370 (2000)

[16] K. Penc, M. Mambrini, P. Fazekas, F. Mila, Phys. Rev. B, **68,** 012408

[17] S. Sorella, G. Santoro, F. Becca, *Sissa lecture notes on Numerical methods for stongly correlated electrons (2005)*

[18] F. Becca, *Electronic properties driven by strong correlation* Thesis (2000)

[19] A. Mishra, M. Ma, Fu-Chun Zhang, Phys. Rev. B, **65,** 214411

[20] M. van den Bossche, P. Azaria, P/ Lecheminant, F. Mila, Phys. Rev. Lett. **86**,18 (2001)

[21] Shun-Qing Shen, Phys. Rev. B **66**, 214516 (2002)

[22] R. Moessner, S. L. Sondhi, P. Chandra, Phys. Rev. B, **64**, 144416 (2001)